ANNUAL REVIEWS

Annual Review of Marine Science

Natural and Anthropogenic Drivers of Acidification in Large Estuaries

Wei-Jun Cai,[1] Richard A. Feely,[2] Jeremy M. Testa,[3] Ming Li,[4] Wiley Evans,[5] Simone R. Alin,[2] Yuan-Yuan Xu,[6,7] Greg Pelletier,[8] Anise Ahmed,[9] Dana J. Greeley,[2] Jan A. Newton,[10] and Nina Bednaršek[8]

[1]School of Marine Science and Policy, University of Delaware, Newark, Delaware 19716, USA; email: wcai@udel.edu

[2]Pacific Marine Environmental Laboratory, National Oceanic and Atmospheric Administration, Seattle, Washington 98115, USA

[3]Chesapeake Biological Laboratory, University of Maryland Center for Environmental Science, Solomons, Maryland 20688, USA

[4]Horn Point Laboratory, University of Maryland Center for Environmental Science, Cambridge, Maryland 21613, USA

[5]Hakai Institute, Heriot Bay, British Columbia V0P 1H0, Canada

[6]Cooperative Institute for Marine and Atmospheric Studies, University of Miami, Miami, Florida 33149, USA

[7]Atlantic Oceanographic and Meteorological Laboratory, National Oceanic and Atmospheric Administration, Miami, Florida 33149, USA

[8]Department of Biochemistry, Southern California Coastal Water Research Project, Costa Mesa, California 92626, USA

[9]Washington State Department of Ecology, Olympia, Washington 98504, USA

[10]Applied Physics Laboratory and Washington Ocean Acidification Center, University of Washington, Seattle, Washington 98105-6698, USA

Annu. Rev. Mar. Sci. 2021. 13:23–55

First published as a Review in Advance on September 21, 2020

The *Annual Review of Marine Science* is online at marine.annualreviews.org

https://doi.org/10.1146/annurev-marine-010419-011004

Keywords

ocean acidification, OA, estuarine biogeochemistry, carbon cycle, acidification sensitivity, buffer factors, maximum estuarine acidification zone, future changes of carbonate chemistry, OA impacts on coastal calcifiers

Abstract

Oceanic uptake of anthropogenic carbon dioxide (CO_2) from the atmosphere has changed ocean biogeochemistry and threatened the health of

organisms through a process known as ocean acidification (OA). Such large-scale changes affect ecosystem functions and can have impacts on societal uses, fisheries resources, and economies. In many large estuaries, anthropogenic CO_2-induced acidification is enhanced by strong stratification, long water residence times, eutrophication, and a weak acid–base buffer capacity. In this article, we review how a variety of processes influence aquatic acid–base properties in estuarine waters, including coastal upwelling, river–ocean mixing, air–water gas exchange, biological production and subsequent aerobic and anaerobic respiration, calcium carbonate ($CaCO_3$) dissolution, and benthic inputs. We emphasize the spatial and temporal dynamics of partial pressure of CO_2 (pCO_2), pH, and calcium carbonate mineral saturation states. Examples from three large estuaries—Chesapeake Bay, the Salish Sea, and Prince William Sound—are used to illustrate how natural and anthropogenic processes and climate change may manifest differently across estuaries, as well as the biological implications of OA on coastal calcifiers.

1. INTRODUCTION

Since the beginning of the Industrial Revolution, the world ocean has taken up approximately 26% of the anthropogenic carbon dioxide (CO_2) humans have released into the atmosphere (Friedlingstein et al. 2019). This process has acidified seawater through increases in the seawater hydrogen ion concentration ($[H^+]$) and corresponding decreases in pH, carbonate ion concentration ($[CO_3^{2-}]$), and calcium carbonate ($CaCO_3$) mineral saturation state (Ω) and is known as ocean acidification (OA) (Bates et al. 2012, 2014; Brewer 2009; Caldeira & Wickett 2003; Doney et al. 2009, 2020; Feely et al. 2004, 2009; Orr et al. 2005; Takahashi et al. 2014). Active OA research over the past two decades has improved our understanding of the mechanisms controlling the spatial patterns and temporal variability of global ocean carbonate chemistry (L.-Q. Jiang et al. 2015, 2019; Takahashi et al. 2014; Völker et al. 2002) and has revealed how ocean chemistry [e.g., partial pressure of CO_2 (pCO_2), pH, and Ω] (Kwiatkowski & Orr 2018, Landschützer et al. 2018, McNeil & Sasse 2016, Perez et al. 2018) and marine organisms (Albright et al. 2018, Riebesell & Gattuso 2014, Waldbusser et al. 2015a) are responding to anthropogenic CO_2 uptake.

Coastal ocean OA studies have particularly focused on how anthropogenic CO_2-induced acidification is mitigated and exacerbated, respectively, by biological production in surface waters and subsequent respiration in subsurface waters as a result of natural nutrient enrichment or human-induced coastal eutrophication (Cai et al. 2011, Feely et al. 2010, Hagens et al. 2015, Sunda & Cai 2012, Van Dam & Wang 2019, Wallace et al. 2014). OA studies in coastal waters have also shown how various economically important wild or cultured organisms—and the ecosystems they reside in—respond to OA and other stressors (e.g., rising temperatures and increasing hypoxia) in coastal and estuarine waters (Bednaršek et al. 2020a, Hales et al. 2016, Waldbusser & Salisbury 2014) and how the aquaculture industry has worked to adapt to changing OA conditions (Barton et al. 2015, Ekstrom et al. 2015, Saba et al. 2019). Because of the strong cultural, economic, and recreational dependencies on such organisms, local governments have reacted with action plans to further assess status, understand drivers, and evaluate adaptation strategies (Adelsman & Binder 2012, Chan et al. 2016). Management strategies will require adequate understanding of underlying drivers in order to be effective.

The dynamics of OA in large estuaries are influenced by a suite of linked external forces and associated internal biogeochemical processes (**Figure 1**). Estuaries and bays are fundamentally defined by the seasonality and magnitude of freshwater inputs and the impact of these forces on physical and chemical gradients. Freshwater inputs deliver poorly buffered water to estuaries, making them vulnerable to OA, but fresh waters are often high in pCO_2 and can lead to outgassing in

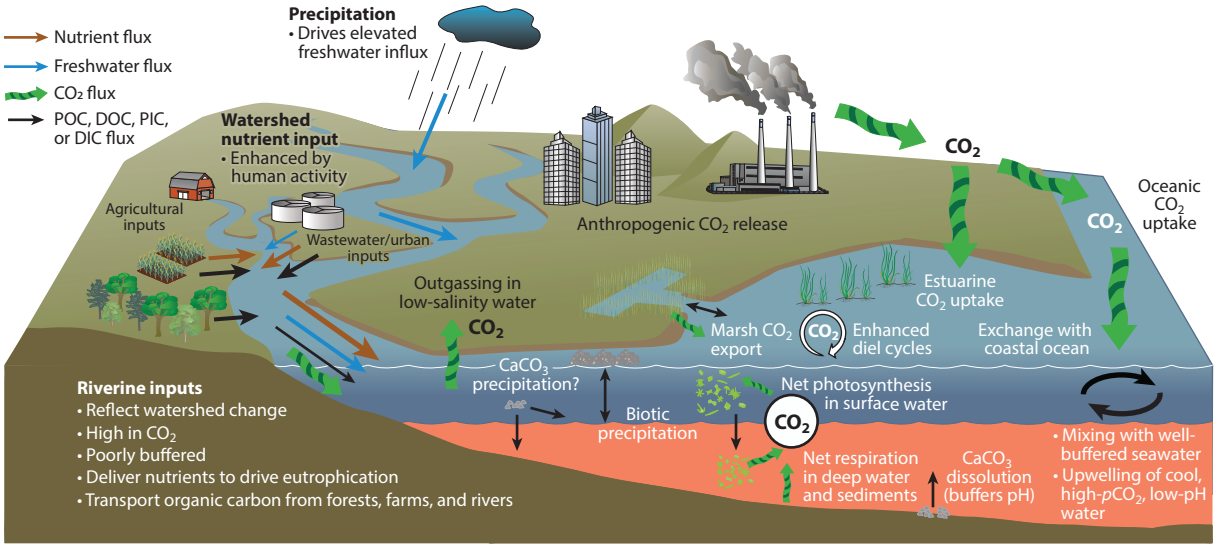

Figure 1

Controlling processes and key dynamics in estuarine carbonate chemistry. Precipitation in the drainage basin enhances the delivery of poorly buffered fresh water to the estuary. Freshwater inputs are often enriched in CO_2 and contribute to CO_2 outgassing in low-salinity regions. Fresh waters can also carry nutrients from perturbed watersheds, leading to eutrophication that enhances CO_2 uptake in surface waters with enhanced primary production but leads to elevated CO_2 production and acidification in deeper waters, where net respiration dominates. Eutrophication-induced bottom-water acidification can conspire with elevated CO_2 uptake from the atmosphere in both the offshore ocean and large estuaries due to the increasing fossil emissions to drive additional acidification. Alternatively, $CaCO_3$ precipitated in productive macrophyte beds or in water-column algal communities or turbidity maxima can be transported to deeper, corrosive waters, where its dissolution buffers against deepwater pH declines. In nearshore waters, wetlands may export high-CO_2 waters, or macrophyte-dominated communities (e.g., seagrasses) can enhance diel pH and CO_2 cycling via extremely high productivity and respiration. At the seawater end member, exchange with relatively well-buffered seawater (though already modified by ocean acidification) can modulate changes in pH associated with watershed effects, while upwelling of cool, low-pH, high-CO_2 water can enhance acidification. Abbreviations: DIC, dissolved inorganic carbon; DOC, dissolved organic carbon; PIC, particulate inorganic carbon; POC, particulate organic carbon.

low-salinity regions (Borges & Abril 2011; Shen et al. 2019a,b). Because estuaries are often associated with population centers due to their abundant biological, aquaculture, and tourism resources, fresh waters draining coastal watersheds may deliver large amounts of inorganic and organic nutrients to tidal waters. Such high-nutrient inputs can lead to eutrophication and, when combined with the vertical stratification that is also driven by freshwater inputs, can cause large vertical and horizontal gradients in carbonate system parameters, pH, dissolved oxygen, and reduced solutes (NH_4^+ and H_2S) (Lee et al. 2015, Zopfi et al. 2001). Thus, the strong seasonality of freshwater input can promote substantial intra-annual variability in the carbonate system. Finally, in some estuaries, benthic processes, tidal wetlands, and submerged aquatic vegetation can contribute substantially to carbonate system dynamics on timescales ranging from hours to years (Cai et al. 1999, Pacella et al. 2018, Su et al. 2020a, Waldbusser & Salisbury 2014).

In this article, we compare the drivers of acidification in large estuaries of the North American Atlantic and Pacific coasts, focusing on the influences of riverine input, buffer capacity, and eutrophication on present and future chemical changes and potential biological impacts of various economically and ecologically important calcifiers. This analysis has value for understanding management and adaptation strategies but also highlights fundamental differences in estuarine carbonate chemistry and their implications for measuring and understanding OA effects.

2. CARBONATE CHEMISTRY IN ESTUARINE WATERS

2.1. Equilibrium Reactions and Their Temperature and Salinity Dependencies

pH is a measure of the hydrogen ion (H^+) activity on a logarithmic scale in aqueous systems. In practice, pH determination is referenced to a set of Standard Reference Materials, which are certified using a primary measurement based on an ideal electrochemical cell and on an internationally agreed-upon convention for single-ion activity coefficients by the US National Institute of Standards and Technology (formerly known as the National Bureau of Standards; here we refer to this convention as the NBS pH scale or pH_{NBS}) (Bates 1973, Baucke 2002, Buck et al. 2002). Marine chemists prefer to define pH on a total H^+ concentration scale: $pH_T = -\log_{10}([H^+] + [HSO_4^-])$ (Dickson 1993, Dickson et al. 2016). The total scale, pH_T, is popularly adopted by our community even though estuarine waters are not a simple dilution of seawater. A spectrophotometric pH measurement method based on a pH-sensitive dye has been established (Clayton & Byrne 1993) and recently extended into low-salinity waters (Müller & Rehder 2018). This method is highly accurate to salinity as low as 5 (Z.-P. Jiang et al. 2019). Further work is still needed to provide a clear theoretical foundation for the definition of pH_T in estuarine waters, and practical analytical methods and Standard Reference Materials are still being developed (Dickson et al. 2016).

In general, pH_T is approximately 0.1–0.15 units lower than pH_{NBS} in seawater, as calculated via the CO2SYS program (Lewis & Wallace 1998, Pierrot et al. 2006). In estuarine waters, the relationship between pH_T and pH_{NBS} is not well known, as the pH scale conversion formula in CO2SYS is not defined for waters with a salinity less than 20. In addition, it is widely reported that pH is inversely and linearly correlated with pCO_2 in seawater (Fassbender et al. 2018); in an estuary, however, the relationship is more curvilinear because of the large changes in the carbonate composition and thermodynamic constants during river–ocean mixing.

Two other basic carbonate chemistry parameters are total dissolved inorganic carbon concentration (DIC, C_T, or TCO_2) and total alkalinity (TA or A_T). DIC is the sum of all the dissolved inorganic carbon species (CO_{2aq}, H_2CO_3, HCO_3^-, and CO_3^{2-}). TA is defined as the excess base in the system, or, in turn, operationally defined as the amount of hydrochloric acid needed to titrate a system to below the CO_2 equivalence point (at a pH of approximately 4.5) (Dickson 1993):

$$\begin{aligned} TA = {} & [HCO_3^-] + 2[CO_3^{2-}] + [OH^-] - [H^+] - [HSO_4^-] \\ & + [B(OH)_4^-] + 2[PO_4^{3-}] + [HPO_4^{2-}] - [H_3PO_4] \\ & + [SiO(OH)_3^-] + [HS^-] + [NH_3] + \text{organic alkalinity}\ldots. \end{aligned} \quad 1.$$

In many of the world's large estuaries, hypoxic and anoxic conditions develop in bottom water, either naturally or through eutrophication. In such cases, CO_2 calculation software with $[HS^-]$ and $[NH_3]$ built into its TA definition should be used (Hofmann et al. 2010, Xu et al. 2017). As a consequence, adding $HgCl_2$ to preserve these samples for TA analysis may lead to the precipitation of HgS_2, releasing acid (Cai et al. 2017, Millero 1991). Thus, a timely analysis of filtered unpreserved water soon after sample collection is necessary (Su et al. 2020a). Another problematic issue in using TA as an input in the CO2SYS program is the unknown contribution of organic acids and bases to TA (i.e., organic alkalinity), as the composition of dissolved organic carbon is highly variable and the content can be high in estuarine waters (Cai et al. 1998, Hunt et al. 2011, Song et al. 2020).

In estuarine and ocean water, there are three primary net reactions involving the carbonate system that regulate the pCO_2, pH, and Ω of the water: gas equilibrium,

$$CO_{2gas} \overset{K_0}{\longleftrightarrow} CO_{2aq}; \quad 2.$$

net acid–base equilibrium,

$$CO_{2aq} + H_2O + CO_3^{2-} \overset{K_1/K_2}{\longleftrightarrow} 2HCO_3^{-}; \quad 3.$$

and mineral dissolution and formation,

$$CaCO_3 + CO_{2aq} \overset{K_{sp}K_1/K_2}{\longleftrightarrow} Ca^{2+} + 2HCO_3^{-}. \quad 4.$$

Here, K_0 is the CO_2 gas solubility constant, and by convention, dissolved aqueous CO_2 (CO_{2aq}, approximately 99.5%) and carbonic acid, H_2CO_3 (approximately 0.5%), are not differentiated and are expressed as a combined term, $[CO_2^*] = [CO_{2aq}] + [H_2CO_3]$ (hereafter $[CO_{2aq}]$, $[CO_2]$, or $[H_2CO_3]$). The first carbonic acid dissociation reaction step is

$$H_2CO_3 \overset{K_1}{\longleftrightarrow} H^+ + HCO_3^{-}, \quad 5.$$

with its equilibrium constant defined as $K_1 = [H^+][HCO_3^-]/[H_2CO_3]$, whereas the second dissociation step is

$$HCO_3^{-} \overset{K_2}{\longleftrightarrow} H^+ + CO_3^{2-}, \quad 6.$$

with its equilibrium constant defined as $K_2 = [H^+][CO_3^{2-}]/[HCO_3^-]$. Thus, K_1/K_2 is the combined constant for the net acid–base reaction in seawater (Equation 3). Finally, Equation 4 is a combination of the calcium carbonate mineral dissolution and precipitation,

$$CaCO_3 \overset{K_{sp}}{\longleftrightarrow} Ca^{2+} + CO_3^{2-}, \quad 7.$$

and the net acid–base reaction (i.e., Equation 4 = Equation 7 + Equation 3). Thus, $CaCO_3$ mineral precipitation will release CO_{2aq}, and dissolution will consume CO_{2aq}. Here, K_{sp} is the apparent solubility constant of a carbonate mineral aragonite or calcite ($K_{sp} = ([Ca^{2+}][CO_3^{2-}])_{equilibrium}$). A mineral saturation state can thus be defined as $\Omega = [Ca^{2+}][CO_3^{2-}]/K_{sp}$. Since the ratio $K_{sp\text{-}aragonite}/K_{sp\text{-}calcite}$ is nearly invariant at constant temperature (1.5 at 25°C; Mucci 1983), in this article, we focus on the saturation state of the more soluble aragonite, Ω_{arag}, the mineral form most commonly incorporated into the shells and hard parts of corals and many other coastal marine organisms, including mollusks.

The thermodynamic constants of the CO_2 system are sensitive to temperature and salinity changes. In coastal waters, temperature and salinity can vary substantially both seasonally and spatially within a given system and across estuaries located at different latitudes or on different ocean margins. In particular, the salinity range can be as large as 0–35 within a single system at any particular time, while the annual water temperature range can be quite wide (>20°C) in many temperate estuaries.

From **Figure 2*a***, it is clear that the CO_2 solubility constant increases as temperature decreases, and thus more CO_2 can dissolve in cold water under the same atmospheric pCO_2 (Equation 2). At the same time, because K_1/K_2 also increases when temperature decreases, low temperature also favors the net acid–base equilibrium shift toward the right, converting CO_2 and CO_3^{2-} to HCO_3^- in Equation 3. But as K_0 is more sensitive than K_1/K_2 to temperature changes, not only will a cold-water body in equilibrium or partial equilibrium with the atmosphere hold more CO_2 and DIC, but its CO_2/DIC fraction will also be higher than that of warm water. Because gas exchange is a slow process (with a timescale of at least one month, depending on the mixed-layer depth) and chemical equilibrium is nearly instantaneous, during a cooling process, $[CO_2]$ may first decrease and then increase, while $[CO_3^{2-}]$ will decrease (Equation 3), and thus Ω_{arag} will decrease too (Cai et al. 2020, Feely et al. 2018). The latter is further aided by a slight increase in $K_{sp\text{-}arag}$ at lower temperatures.

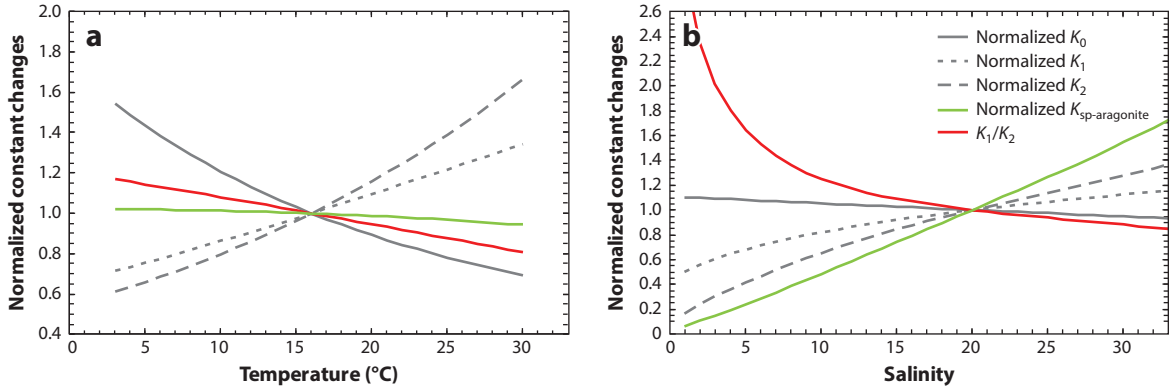

Figure 2

Thermodynamic constants as a function of (*a*) temperature or (*b*) salinity. In panel *a*, all constants are scaled or normalized to a temperature of 16°C [i.e., as $K(T)/K(T = 16°C)$] and a salinity of 35. In panel *b*, all constants are scaled or normalized to a salinity of 20 [i.e., as $K(S)/K(S = 20)$] and a temperature of 25°C. Since these thermodynamic constant changes are presented as normalized values to a midpoint value for illustration purposes, panel *a* is not particularly sensitive to the chosen salinity (results for a salinity of 5 are similar to those for a salinity of 35), and panel *b* is not particularly sensitive to the chosen temperature.

When salt content (salinity) decreases, the solubility of CO_2 in water increases slightly and the dissociation of carbonic acid decreases, primarily due to declines in the second dissociation constant, leading to a sharp increase in the K_1/K_2 ratio (**Figure 2*b***). This is why TA and DIC values in freshwater systems are generally lower than those in the ocean (as less CO_2 will dissociate into HCO_3^- and CO_3^{2-}) and why DIC roughly equals TA (as less HCO_3^- dissociates into CO_3^{2-}, and thus more DIC stays as HCO_3^- and CO_2) in fresh waters. As a result, the DIC/TA ratio is generally higher in fresh water than in salt water, and consequently, carbonate ion supersaturation and mineral precipitation in fresh water require a very high pH (Su et al. 2020a). Since both K_0 and K_1/K_2 increase at lower salinity and lower temperature, estuarine and coastal waters in cold northern regions are expected to have a higher DIC/TA ratio, a lower $[CO_3^{2-}]$, and a weakened ability to withstand CO_2 addition from anthropogenic sources or biological processes (Cai et al. 2020, Feely et al. 2018, Sunda & Cai 2012).

2.2. Sensitivities of Estuarine Waters to Acidification

In an aquatic system, pH change can be deconstructed into component increases or decreases due to changes in temperature, salinity, DIC, and TA:

$$\mathrm{dpH} = \left(\frac{\partial \mathrm{pH}}{\partial \mathrm{T}}\right)\mathrm{dT} + \left(\frac{\partial \mathrm{pH}}{\partial \mathrm{S}}\right)\mathrm{dS} + \left(\frac{\partial \mathrm{pH}}{\partial \mathrm{DIC}}\right)\mathrm{dDIC} + \left(\frac{\partial \mathrm{pH}}{\partial \mathrm{TA}}\right)\mathrm{dTA} + \ldots. \qquad 8.$$

Here, the first and second terms represent the effects of changes in thermodynamic constants as a function of temperature (T) and salinity (S). The slope of the third term is the sensitivity factor ($SF_{\mathrm{DIC}}^{\mathrm{pH}}$) of pH change when DIC is altered, and the slope of the fourth term reflects the pH change sensitivity when a strong acid (H^+ or –TA) is added ($SF_{\mathrm{TA}}^{\mathrm{pH}}$). In seawater, where salinity changes are generally small and due primarily to the net balance of precipitation and evaporation, it is useful to account for the DIC and TA changes that result from biogeochemically induced changes using salinity-normalized terms (Landschützer et al. 2018). However, it is questionable whether such an approach is effective in estuarine and coastal waters, where river end members often contain large and variable DIC and TA (Cai et al. 2008).

The sensitivity factors of pH to changes of DIC or TA in Equation 8 are directly related to the acid–base buffer factors β_{DIC} and β_{TA} (Egleston et al. 2010, Frankignoulle 1994):

$$\beta_{DIC} = \left(\frac{1}{[H^+]}\frac{\partial [H^+]}{\partial DIC}\right)^{-1} = \left(\frac{\partial \ln [H^+]}{\partial DIC}\right)^{-1} = -\left(2.3\frac{\partial pH}{\partial DIC}\right)^{-1} \quad 9.$$

and

$$\beta_{TA} = \left(\frac{1}{[H^+]}\frac{\partial [H^+]}{\partial TA}\right)^{-1} = \left(\frac{\partial \ln [H^+]}{\partial TA}\right)^{-1} = -\left(2.3\frac{\partial pH}{\partial TA}\right)^{-1}. \quad 10.$$

Since the buffer factor is defined as the inverse of the fractional sensitivity of $[H^+]$, its unit is the same as the unit for DIC and TA (μmol kg^{-1}) (Álvarez et al. 2014), and thus the unit for the sensitivity factor is (μmol kg^{-1})$^{-1}$. Similarly, the sensitivity of pCO_2 to temperature, salinity, DIC ($SF_{DIC}^{CO_2}$), and TA changes can be defined with their respective sensitivity coefficients linked to the previously defined buffer factors (Takahashi et al. 1993), including

$$\gamma_{DIC} = \left(\frac{1}{[CO_2]}\frac{\partial [CO_2]}{\partial DIC}\right)^{-1} = \left(\frac{\partial \ln [CO_2]}{\partial DIC}\right)^{-1} \quad 11.$$

and a related, popularly used sensitivity factor, the Revelle factor, defined as

$$\left(\frac{\partial pCO_2}{pCO_2} \Big/ \frac{\partial DIC}{DIC}\right) = \frac{\partial \ln [CO_2]}{\partial \ln DIC} = \frac{DIC}{\gamma_{DIC}}. \quad 12.$$

Since the Revelle factor is the fractional sensitivity of pCO_2 to the fractional DIC change, it is dimensionless. Similarly, the sensitivity of CO_3^{2-} and Ω to DIC change can also be defined with its component sensitivity linking to the buffer factor:

$$\omega_{DIC} = \left(\frac{1}{\left[CO_3^{2-}\right]}\frac{\partial \left[CO_3^{2-}\right]}{\partial DIC}\right)^{-1} = \left(\frac{\partial \ln \left[CO_3^{2-}\right]}{\partial DIC}\right)^{-1} = \left(\frac{\partial \ln \Omega}{\partial DIC}\right)^{-1}. \quad 13.$$

Since $[Ca^{2+}]$ and K_{sp} do not change under constant temperature and salinity, the buffer and sensitivity factors are the same for the carbonate ion and saturation states of aragonite and calcite minerals. (For a more comprehensive treatment of acid–base sensitivity factors in seawater, see Middelburg et al. 2020.)

The three sensitivity factors, SF_{DIC}^{pH}, $SF_{DIC}^{CO_2}$, and $SF_{DIC}^{CO_3^{2-}}$, are plotted in **Figure 3**. It is clear that low-salinity estuarine waters are much more sensitive to DIC increases than seawater, where changes in pH and fractional changes in pCO_2 and CO_3^{2-} or Ω_{arag} are larger for a given DIC input. There are also subtle differences, in that pCO_2 and pH are more sensitive than CO_3^{2-} and Ω_{arag} to DIC changes at all salinities. However, in estuarine conditions, because the DIC- and TA-induced buffer or sensitivity factors are generally similar in magnitude (Egleston et al. 2010) (**Figure 3**), the overall contributions to acidification or pH decreases are decided largely by the changes in DIC and TA during gas exchange and biogeochemical processes (e.g., at constant temperature and salinity) and also by the initial buffering capacity (e.g., initial DIC and TA at the given temperature and salinity).

From **Figure 3**, it is also clear that the pH (or pCO_2 and Ω_{arag}) sensitivity of an estuarine water mass can differ greatly depending on the TA value of the river end member. This is because the river DIC/TA ratio of approximately 1.0 is modified toward the seawater level of approximately 0.87 much more rapidly in estuaries receiving low-TA rivers than those receiving high-TA rivers. Thus, in the low-salinity zone, estuaries receiving low-TA rivers show higher sensitivity to CO_2 addition than estuaries receiving high-TA rivers. This feature of a higher and rapidly changing

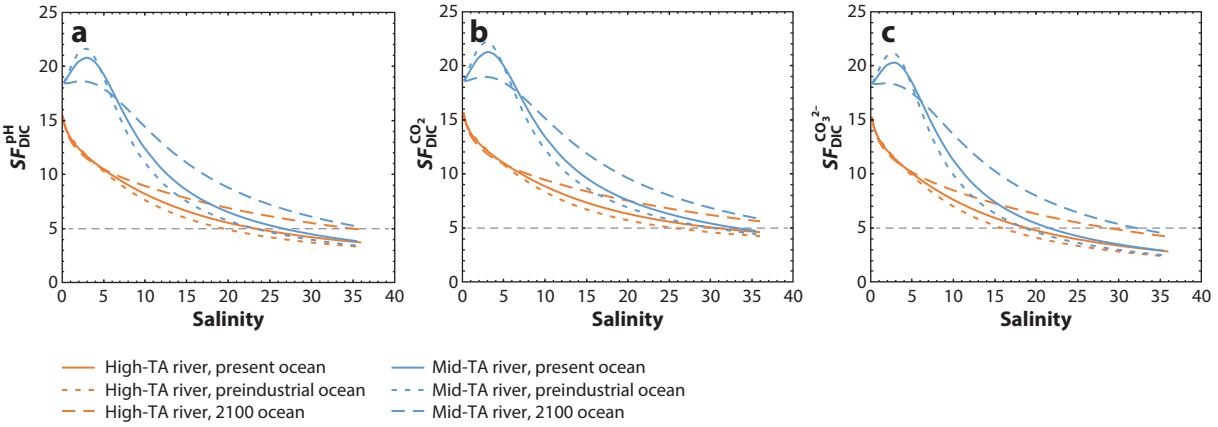

Figure 3

Sensitivity factors in terms of fractional change of a species per unit of DIC modification in estuaries. To be comparable, all three are presented as the inverse of their respective buffer factors: (*a*) $SF_{DIC}^{pH} = (\beta_{DIC})^{-1} = \left(\frac{1}{[H^+]}\frac{\partial[H^+]}{\partial DIC}\right) = -2.3\frac{\partial pH}{\partial DIC}$, (*b*) $SF_{DIC}^{CO_2} = (\gamma_{DIC})^{-1} = \left(\frac{1}{[CO_2]}\frac{\partial[CO_2]}{\partial DIC}\right)$, and (*c*) $SF_{DIC}^{CO_3^{2-}} = (-\omega_{DIC})^{-1} = \left(-\frac{1}{[CO_3^{2-}]}\frac{\partial[CO_3^{2-}]}{\partial DIC}\right)$. Two river alkalinity levels are simulated with a high-TA river (e.g., the Mississippi) and a mid-TA river (e.g., the Susquehanna, which feeds into Chesapeake Bay). The DIC modifications are simulated as anthropogenic CO_2 addition from the preindustrial era (air CO_2 = 280 ppm), the present (air CO_2 = 390 ppm), and the year 2100 (assuming air CO_2 = 800 ppm). Abbreviations: DIC, dissolved inorganic carbon; TA, total alkalinity. Figure adapted with permission from Cai et al. (2017).

sensitivity in low-TA estuaries can have important implications for estuarine pH distributions and the effects of CO_2 addition on pH and Ω_{arag} decreases (see Section 3.1). However, in these poorly buffered waters, the sensitivity and buffer factors can be readily modified by net biological production (Cai et al. 2020).

3. IMPACTS OF ESTUARINE PROCESSES ON CARBONATE CHEMISTRY AND ACIDIFICATION

Surface-water distributions of pCO_2, pH, TA, DIC, and Ω_{arag} in large estuaries are influenced by a wide variety of processes (**Figure 1**), with varying degrees of importance in different estuaries. External drivers include river and wetland inputs, oceanic inputs, and anthropogenic CO_2 uptake, while internal drivers include estuarine circulation, vertical and lateral mixing, spatial and seasonal temperature variations, the balance of biological production and respiration, $CaCO_3$ precipitation and dissolution, and inputs from benthic respiration. Rivers typically deliver water to estuaries that is more acidified and has a higher DIC/TA ratio than that of seawater and may thus weaken the ability of estuarine waters to withstand anthropogenic CO_2-induced acidification (Huang et al. 2015, Salisbury et al. 2008). However, increased nutrient input from rivers may lead to elevated biological CO_2 removal and consequent basification and increased buffer capacity in surface waters (Borges & Gypens 2010), whereas enhanced acidification and decreased buffer capacity (or increased pH sensitivity) may occur in bottom waters, where biogenic materials are ultimately respired and CO_2 is released back into the water column (Cai et al. 2011). Estuaries that are well mixed will attenuate these depth differences in carbonate chemistry, and those that are strongly stratified will accentuate them (Cai et al. 2017). Moreover, in estuaries receiving significant freshwater inputs, Ω_{arag} can also be suppressed by reduced $[Ca^{2+}]$ and $[CO_3^{2-}]$ in the very-low-salinity

zone. Finally, coastal upwelling can bring low-pH and low-Ω_{arag} waters into deep bays, where respiration can further reduce pH and Ω_{arag} (Feely et al. 2008, 2010, 2016).

3.1. River–Ocean Mixing and Water Residence Time

In stratified large estuaries receiving substantial freshwater input, such as Chesapeake Bay, salinity-induced stratification is strong, but turbulent mixing can also be important under the right combination of wind and tidal mixing processes (Geyer & MacCready 2014, Goodrich et al. 1987, Scully et al. 2005, Xie & Li 2018), resulting in a partially stratified system with strong seasonal variations. In some large, deep estuaries formed by glaciers, such as large portions of the Salish Sea, there is near-permanent stratification, with little vertical mixing into the deeper water except during the winter months in some cases (Evans et al. 2019, Feely et al. 2010). Both types of estuaries have long water residence times (Du & Shen 2016, Sutherland et al. 2011), as do other deep estuarine basins (e.g., the Baltic Sea). Sharp spatial differences can also occur along estuarine channels; large estuaries along the US east coast (e.g., Chesapeake and Delaware Bays) often have a river–ocean mixing zone with rapidly changing salinity and biogeochemistry in the upper estuary that then gives way to a seaward bay region characterized by less dynamic salinity and biogeochemistry (Sharp 2010, Sharp et al. 2009, Sommerfield & Wong 2011). For example, in the upper Chesapeake and Delaware Bays and tributaries, pCO_2 is high, and its distribution and variation are similar to those of many small estuaries reported in Europe (Borges & Abril 2011) and the southeastern United States (Cai 2011, Cai & Wang 1998), while in the lower bays, pCO_2 is low and is near atmospheric equilibrium, reflecting features of a eutrophic large bay and its offshore waters (Herrmann et al. 2020, Joesoef et al. 2015, Shen et al. 2019a, St-Laurent et al. 2020).

While CO_2 uptake in surface waters of the open ocean increases DIC and thus the DIC/TA ratio (Feely et al. 2009, 2012b; L.-Q. Jiang et al. 2019), we assume that anthropogenic CO_2 does not appreciably change the river end-member DIC/TA ratio and that the signal of oceanic uptake of anthropogenic CO_2 is transferred into estuarine waters through mixing with river waters (Hu & Cai 2013). We make this latter assumption because most rivers have a high DIC/TA ratio relative to the ocean and a supersaturated pCO_2 with respect to the atmosphere (Borges & Abril 2011, Cai 2011). However, the impact of anthropogenic CO_2 on estuarine acidification can, in fact, depend on the incoming river TA values, as discussed in Section 2.2. The complex interactions of mixing are relevant because TA values are highly variable among the world's rivers; these interactions are controlled mainly by the carbonate mineral contents and net precipitation in their drainage basins, as is the extent of river and ocean water mixing (Cai et al. 2008). For example, large tropical rivers, such as the Amazon and Orinoco in South America, and regional rivers, such as the Altamaha and Savannah in the southeastern United States, have TA values as low as 300–500 $\mu mol\ kg^{-1}$, whereas large rivers in subtropical and middle latitudes, such as the Mississippi in the United States and the Changjiang (Yangtze) and Huanghe (Yellow River) in China, have high TA values of 1,800–3,500 $\mu mol\ kg^{-1}$ (Cai et al. 2008, 2010a). Major rivers that feed into the large estuaries on the US east coast, such as the Susquehanna and Delaware Rivers, have TA values of approximately 1,000 $\mu mol\ kg^{-1}$, which is similar to the global river average TA (Brodeur et al. 2019, Cai & Wang 1998, Joesoef et al. 2017).

As a consequence, when river TA is high (e.g., the Mississippi River) and the associated buffering capacity is strong over the entire salinity range, pH changes induced by anthropogenic CO_2 are relatively small and are proportional to the open-ocean OA source signal, which decreases toward zero salinity (**Figure 4**). By contrast, when river TA values are low or intermediate (e.g., the Altamaha or Susquehanna Rivers), pH sensitivity is high in the very-low-salinity waters, but sensitivity decreases rapidly toward high salinity. In this case, the oceanic OA signal is amplified

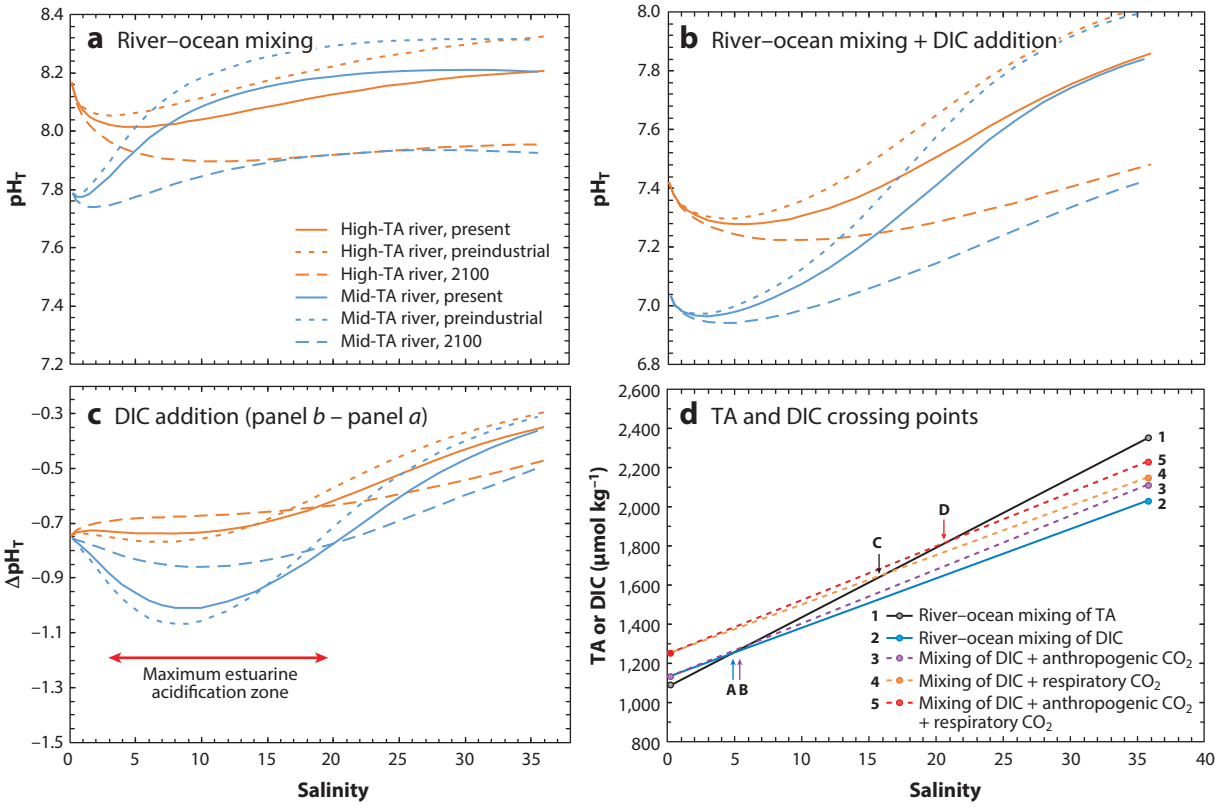

Figure 4

Simulations of pH_T (25°C) changes in response to estuarine mixing and DIC additions from anthropogenic and biological sources in two large estuaries, one with a high-TA river (e.g., Mississippi River coastal waters) (*orange*) and one with a mid-TA river (e.g., Chesapeake Bay waters) (*blue*). (*a*) pH_T curves during estuarine mixing under three scenarios (present day, preindustrial era, and year 2100). (*b*) pH_T curves plus full O_2 consumption (respiration) during estuarine mixing. (*c*) pH_T decrease (ΔpH_T) as a result of full O_2 consumption during estuarine mixing (the difference between panel *b* and panel *a*). Note that the scenario in panel *b* does not match that from the real data at low salinities, because a stratified and O_2-depleted state does not exist for the very-low-salinity part of Chesapeake Bay due to strong mixing. (*d*) Estuarine TA mixing line between the river and ocean end members and DIC mixing lines with additional CO_2 added from anthropogenic sources and respiration. The TA line (line 1) crosses the DIC lines (lines 2, 3, 4, and 5) at points A, B, C, and D, respectively. Abbreviations: DIC, dissolved inorganic carbon; TA, total alkalinity. Figure adapted with permission from Cai et al. (2017).

in zones with low TA and low and intermediate salinities (**Figures 3** and **4**). For example, similar amounts of aerobic respiration would lead to a pH decrease of approximately 0.4 units in strongly buffered northern Gulf of Mexico waters (Cai et al. 2011) but a much larger decrease of nearly 0.8 units in the poorly buffered Chesapeake Bay waters (Cai et al. 2017). Interestingly, the combination of an increasing acid–base sensitivity factor (with decreasing salinity) and a strong but decreasing oceanic OA signal generates a minimum buffer zone (Hu & Cai 2013) (**Figure 3**) and thus a maximum estuarine acidification zone (**Figure 4**). For example, this zone occurs at salinities of 2–18 in Chesapeake Bay (Cai et al. 2017). This complexity underscores that OA effects in estuaries are site specific and not generic across all estuaries.

The existence of a maximum estuarine acidification zone and its salinity range depend on the river TA value and the DIC/TA ratio across the estuarine mixing zone. The minimum buffer zone

occurs at an intersection point where the DIC–salinity mixing line crosses the TA–salinity mixing line associated with declines in the DIC/TA ratio as salinity increases (**Figure 4*d***). A maximum estuarine acidification zone will be more apparent and will occur at a higher salinity when more CO_2 is added to the system by microbial respiration, as the DIC = TA crossover point will shift to higher salinity, as illustrated in **Figure 4*d*** (Cai et al. 2017, Hu & Cai 2013). Note that this crossover point occurs where $[CO_3^{2-}] = [CO_2]$ if we ignore $[B(OH)_4^-]$ and other minor species contributing to TA at low pH (see Equation 1). On the higher-salinity side of this point, we have $[CO_3^{2-}] > [CO_2]$, and the system can still convert anthropogenic or biologically produced CO_2 to HCO_3^- (Equation 3), whereas on the lower-salinity side, we have $[CO_3^{2-}] < [CO_2]$, and the system has essentially lost its capacity to buffer CO_2 additions (Egleston et al. 2010, Feely et al. 2018).

3.2. Impacts of Biological Production and Gas Exchange

In addition to river–ocean mixing, estuarine carbonate chemistry, including pH and Ω_{arag}, is also influenced by biological activities and air–sea gas exchange. In recent decades, eutrophication has led to strong biological production in surface waters and severe hypoxia in bottom waters of multiple types of estuaries, including large estuaries, bays, and offshore river plume areas (Fennel & Testa 2019). As a result, surface waters of these estuaries generally have low pCO_2 and serve as CO_2 sinks, particularly during seasons of high biological productivity (spring and summer). This contrasts with the fact that most small and midsize estuaries studied to date are heterotrophic and are sources of CO_2 to the atmosphere (Borges & Abril 2011, Cai 2011). While less studied in the context of OA research, increases of surface-water pH in river plume and estuarine waters have been reported and attributed to eutrophication (Borges & Gypens 2010, Xue et al. 2016). However, numerical model exercises suggest that recent nutrient mitigation has contributed to pH decreases in surface waters of the middle and lower Chesapeake Bay over the past 30 years (Shen et al. 2020).

Acidification caused by local CO_2 exchange with the atmosphere is generally not a concern in most estuaries, as surface-water residence times are not long enough to allow for significant DIC accumulation and most smaller estuaries are already CO_2 supersaturated with respect to the atmosphere. However, in large estuaries—which have a combination of long residence times, low pCO_2 values resulting from strong biological CO_2 uptake, and more ocean-influenced water masses—the local air–sea CO_2 exchange can play a significant role in estuarine acidification. For example, in Chesapeake Bay, because the water residence time is more than 100 days during spring and summer (Du & Shen 2016), low surface-water pCO_2 combined with active tidal mixing (despite vertical stratification) allows for local atmospheric uptake to be mixed to the bottom and allows DIC accumulation of 20–35 $\mu mol\ kg^{-1}$ in the water column, which can substantially reduce bottom-water pH and Ω_{arag} (Cai et al. 2017, Shen et al. 2019a, Su et al. 2020b). These findings are supported by recent numerical model simulations, which have shown that increased atmospheric CO_2 and river nutrient loading are the two dominant drivers for increasing ingassing and decreasing degassing in Chesapeake Bay over the past century (St-Laurent et al. 2020) and in recent decades (Shen et al. 2020).

3.3. Impacts of Microbial Respiration

In aquatic systems, microbial communities oxidize biological products (organic matter), initially using free oxygen and then using bound oxygen (e.g., NO_3^- and SO_4^{2-}), in a sequence of reactions with diminishing net energy gain (Cai et al. 2010b, Hofmann et al. 2009, Wang & Van Cappellen 1996). As aerobic respiration produces CO_2 while slightly decreasing TA, it is generally the most

effective respiration process to reduce water column pH and Ω_{arag}:

$$(CH_2O)_{106}(NH_3)_{16}H_3PO_4 + 138O_2 \rightarrow 106CO_2 + 16HNO_3 + H_3PO_4 + 122H_2O. \quad 14.$$

According to the definition of TA, we have $\Delta TA/\Delta DIC = -(16 + 1)/106 = -0.16$ for aerobic respiration, if the classic Redfield stoichiometry is adopted. Note that here H_3PO_4 would contribute one H^+ (Equation 1).

Denitrification and sulfate reduction only slightly affect the ratio of DIC/TA in water, and thus, under most conditions, they would only moderately affect aquatic pH (Cai et al. 2010b):

$$(CH_2O)_{106}(NH_3)_{16}H_3PO_4 + 0.8 \times 106NO_3^- + 0.8 \times 106H^+ \rightarrow 106CO_2 + 0.4 \times 106N_2 + 16NH_3 + H_3PO_4 + 1.4 \times 106H_2O \quad 15.$$

with $\Delta TA/\Delta DIC = 0.8 + (16 - 1)/106 = 0.94$, and

$$(CH_2O)_{106}(NH_3)_{16}H_3PO_4 + 106/2SO_4^{2-} + 106H^+ \rightarrow 106CO_2 + 106/2H_2S + 16NH_3 + H_3PO_4 + 106H_2O \quad 16.$$

with $\Delta TA/\Delta DIC = 1 + (16 - 1)/106 = 1.14$.

Metal oxide reduction would generate the maximum amount of base per mole of CO_2 production, although its overall role in CO_2 production is generally limited. In most estuaries, including Chesapeake Bay waters, the two most important processes are aerobic respiration and sulfate reduction (Cai et al. 2017, Canfield et al. 1993) (**Figure 5**).

Coastal marine sediments rich in organic matter often exhibit a sharp pH minimum in low-oxygen zones near the oxygen penetration depth in sediment pore waters (Boudreau & Canfield 1993, Cai & Reimers 1993, Cai et al. 2006), which is a result of oxidation of reduced species (mostly

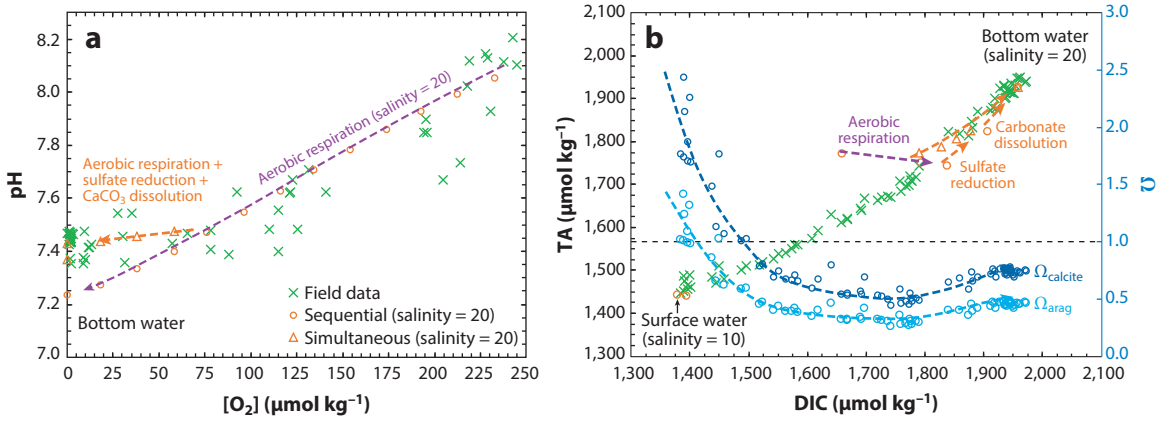

Figure 5

Model simulations of the evolution of pH, O_2, DIC, and TA during biogeochemical processes. Here, pH was measured by a glass electrode on board the ship at 25°C by referencing to a set of NBS standards and is presented as pH_{NBS}, which is roughly 0.1 unit higher than pH_T presented elsewhere in this article. (*a*) Relationship between pH (25°C) and [O_2]. (*b*) Relationship between TA and DIC, with Ω_{arag} and $\Omega_{calcite}$ plotted as the second *y* axis. The biogeochemical pathway (TA and DIC loci) includes aerobic respiration, sulfate reduction, and $CaCO_3$ dissolution. Predicted pH or TA values are provided together with observed pH or TA calculated from pH and DIC data from August 2013 observations. Both sequential (*open circles*) and simultaneous (*triangles*) pathways are presented. In the sequential simulation, we assumed that biogeochemical processes complete in the order of aerobic respiration, sulfate reduction, and $CaCO_3$ dissolution. In the simultaneous simulation, once [O_2] falls below 70 μmol kg^{-1}, $CaCO_3$ dissolution and sulfate reduction are allowed to proceed. Note that in the field, local anoxia and sulfate reduction can occur when average bottom-water [O_2] is still above zero. Abbreviations: DIC, dissolved inorganic carbon; NBS, National Bureau of Standards; TA, total alkalinity. Figure adapted with permission from Cai et al. (2017).

H_2S but also NH_4^+) by oxygen. Here, H_2S and NH_4^+ diffuse upward from deeper sediments, where SO_4^{2-} reduction predominates. The associated acid production reaction ($H_2S + 2O_2 \rightarrow SO_4^{2-} + 2H^+$) could be an important factor regulating bottom-water pH (Hofmann et al. 2009) and a reason for $CaCO_3$ dissolution in sediments (Jensen et al. 2009). While rarely reported, evidence of such a pH minimum in the water column can be gleaned from the literature (Yao & Millero 1995), and H_2S oxidation was recently reported to have caused a pH minimum at the zone where H_2S-containing subsurface anoxic water mixes with oxygen-containing surface waters inside Chesapeake Bay due to tidal turbulence (Cai et al. 2017).

3.4. $CaCO_3$ Mineral Formation and Dissolution

The dynamics of calcification and dissolution are potentially important contributors to DIC and especially TA variability, but little is known about the rate and spatial pattern of these processes outside of communities dominated by calcifiers (e.g., coral and bivalve reefs). Negative feedbacks could exist, where decreasing TA leads to low Ω_{arag} that then drives dissolution that generates TA to buffer against further Ω_{arag} declines. If calcification occurs in a different location from dissolution, there may be local imbalances in TA production and consumption. For example, in Chesapeake Bay bottom water, oxygen and pH decline in tandem during spring and early summer, and Ω_{arag} decreases to very low values of <0.5 (**Figure 5**). Under such conditions, $CaCO_3$ dissolution would serve to buffer the bottom water and stop further pH and Ω_{arag} decreases (Cai et al. 2017). Coupled physical-biological model simulations indicated that from June to August, when oxygen continues to decrease from hypoxia to anoxia, pH and Ω_{arag} no longer decrease but rather increase in association with $CaCO_3$ dissolution (Shen et al. 2019a).

While the origin of the $CaCO_3$ solids to support this dissolution is unclear, it challenges the estuarine research community to identify potential sources of $CaCO_3$ production. Recent work suggests multiple potential pathways. In Chesapeake Bay, nutrient load reductions have recently contributed to resurgent dense, submerged aquatic vegetation beds in shallow waters of some regions, whose intense metabolism greatly elevates pH and Ω_{arag} in the surrounding water, stimulating the formation of $CaCO_3$ solids on leaf surfaces. These solids and other forms of biogenic $CaCO_3$ can be subsequently transported seaward and laterally into the deep, oxygen-deficient, low-pH zones in the middle and lower bay, where the $CaCO_3$ solids react with anthropogenic and metabolic CO_2 and increase TA, thus buffering further pH declines (Su et al. 2020a). Thus, a spatially separated $CaCO_3$ cycle–based pH buffering mechanism may be observed in coastal environments that are experiencing mitigation of eutrophication, reduction of phytoplankton primary production, resurgence of calcifying organisms, and restricted water exchange with the open ocean. For instance, Abril et al. (2003) demonstrated that the authigenic $CaCO_3$ precipitated in the Loire River was closely coupled with intense primary production, while $CaCO_3$ dissolution occurred in the downstream oxygen-deficient estuarine turbidity maximum zone, where net respiration led to low pH and Ω_{arag}. On the other hand, Najjar et al. (2020) posed an alternative pathway, where low-salinity TA sinks were associated with dense bivalve growth.

4. CURRENT AND FUTURE ACIDIFICATION IN LARGE ESTUARIES

Here, we draw on the theoretical foundations established above to apply our understanding of estuarine carbonate chemistry in case studies of select large estuarine systems. Chesapeake Bay is the largest estuary along the US Atlantic coast, while the Salish Sea and Prince William Sound are among the largest estuaries along the US and Canadian Pacific coasts. We focus on the main

features of carbonate chemistry, the associated OA status in these estuaries, their projected changes under climate change scenarios, and the biological implications for calcifiers living there.

4.1. Chesapeake Bay

Chesapeake Bay, located in the mid-Atlantic region of the US east coast, is an example of a large, temperate, coastal plain estuary experiencing both eutrophication and anthropogenic acidification. Its large size, diversity of habitats, and strong chemical and physical gradients make it a useful case study for the diversity of processes driving coastal carbonate chemistry.

4.1.1. Estuarine biogeochemistry and carbonate chemistry. Chesapeake Bay is a large, partially stratified coastal plain estuary that receives fresh water, nutrients, and organic matter from several rivers, the largest of which is the Susquehanna River. Freshwater inputs generate strong seasonal vertical stratification in the bay, gravitational circulation with a mean net inflow in deep waters (Carter & Pritchard 1988, Li et al. 2005), and a mean residence time of 180 days (Du & Shen 2016). Given relatively high surface inputs of poorly buffered water and stratification that isolates deeper waters with high respiration rates (and thus high CO_2 production and accumulation), Chesapeake Bay is vulnerable to OA relative to many other temperate and subtropical coastal zones.

Strong vertical and horizontal oxygen, nutrient, and carbonate chemistry gradients develop seasonally in Chesapeake Bay. In low-salinity waters influenced by fresh water, inputs of high-pCO_2 river water combined with local respiration of terrestrial organic matter inputs and light-limited primary production (which limits CO_2 uptake) lead to substantial accumulations of CO_2 (pCO_2 > 3,000 μatm; Cai et al. 2017, Su et al. 2020b). These patterns also persist in Chesapeake Bay tributaries (Shen et al. 2019b) and in low-salinity waters in other temperate coastal plain estuaries, such as Delaware Bay and Long Island Sound (Joesoef et al. 2015, Wallace et al. 2014). These low-salinity waters are also characterized by low pH and CO_3^{2-} concentrations, by virtue of poor buffering (**Figures 2** and **3**). Moving seaward, surface-water pH and Ω_{arag} increase in association with higher oceanic influence (and thus exchange with waters containing high TA and DIC) and increasing primary production and CO_2 uptake owing to the relief of light limitation under relatively high nutrient levels. Under stratified conditions, high surface-water pH and Ω_{arag} give way to low pH (as low as 7.3), high DIC, and low Ω_{arag} (as low as 0.4; **Figure 5**) in underlying bottom waters that have restricted exchanges with surface water and where respiration enables high rates of CO_2 production. Detailed observations of these spatial patterns and their seasonal variability are described elsewhere (Brodeur et al. 2019; Friedman et al. 2020; Su et al. 2020a,b).

Chesapeake Bay bottom waters with high respiration rates develop hypoxia and anoxia seasonally, and low oxygen and pH combine to alter carbonate system dynamics through several mechanisms. First, anoxia leads to anaerobic metabolism via sulfate reduction and the production and eventual release of hydrogen sulfide (Equation 16, **Figure 5**) in bottom waters and sediments (Roden & Tuttle 1992). Upward fluxes of HS^- and NH_4^+ produced from respiration can cause a midwater minimum in pH where these reduced species are oxidized (Cai et al. 2017). Under northerly (down-estuary) winds, deep water with low oxygen, high CO_2, low pH, and low Ω_{arag} can be upwelled rapidly toward the eastern shore, creating brief (on the order of hours) acidified and hypoxic conditions there (Huang et al. 2019) (**Figure 6**). Similar lateral upwelling can occur on the west side of the bay under southerly (up-estuary) winds (Scully 2010, Xie et al. 2017). Such rapid changes in oxygen and acidification conditions in response to wind (Sanford et al. 1990) could put organisms under high stress. In extreme cases, these conditions would force crabs and fishes to move to shallow, nearshore environments to escape the unfavorable deep waters, resulting

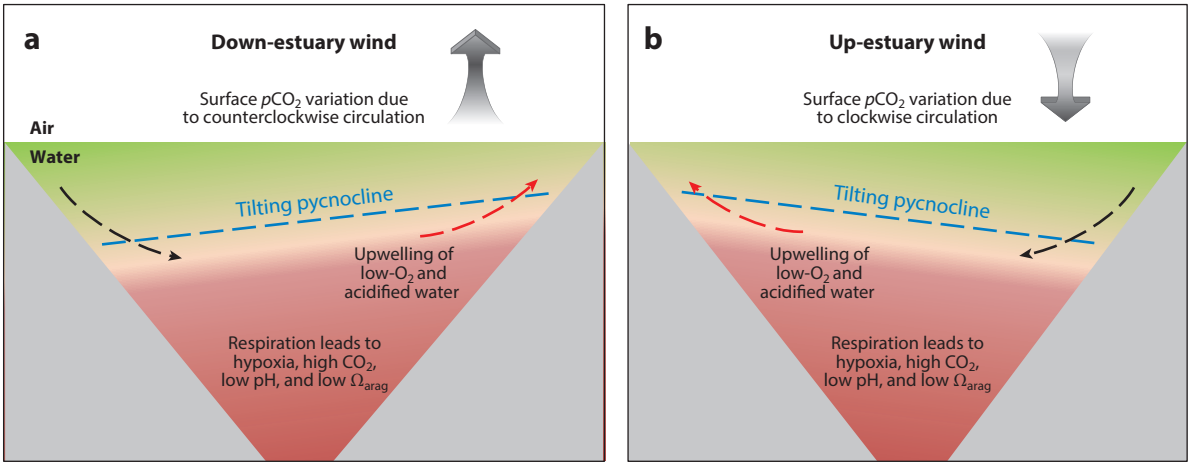

Figure 6

Wind-driven lateral upwelling and its effects on the biogeochemical processes in a stratified estuary. (*a*) Down-estuary or northerly winds (blowing up out of the page, toward the reader) generate a counterclockwise lateral circulation and upwelling on the eastern shore, producing high-pCO_2 and low-pH conditions there. (*b*) Up-estuary or southerly winds (blowing in the opposite direction, away from the reader) produce upwelling and high-pCO_2 and low-pH conditions on the western shore. Both down-estuary and up-estuary winds can produce conditions favorable for releasing respired DIC in the water column. Abbreviations: DIC, dissolved inorganic carbon; pCO_2, partial pressure of CO_2. Figure adapted from Huang et al. (2019).

in so-called jubilees (Loesch 1960, Sanford et al. 1990). The persistence of conditions favorable to carbonate dissolution in these bottom waters also leads to high rates of dissolution, where TA generation (Equation 4) can potentially buffer against additional pH declines during late summer (Shen et al. 2019a) (**Figure 5**). Given the strong seasonal and interannual variability in freshwater inputs, stratification, and extent of low-oxygen bottom water, the relative magnitude of each of these processes in driving carbonate system dynamics varies substantially (Cai et al. 2017; Lee et al. 2015; Shen et al. 2019a,b; Su et al. 2020a).

4.1.2. Future climate projections. With accelerating climate change in the twenty-first century, it is important to predict the future trajectory of estuarine acidification and investigate whether or when the ecological thresholds of marine organisms may be crossed under future climate conditions. To investigate future acidification under climatic change in Chesapeake Bay, a coupled hydrodynamic–biogeochemical–carbonate chemistry model [Regional Ocean Modeling System (ROMS)–Row-Column AESOP (RCA)–Carbonate Chemistry (CC)] (Shen et al. 2019a) was forced with climate downscaling projections from regional and global climate models (Mearns et al. 2013) in an effort to make projections for dissolved oxygen (Ni et al. 2019) and acidification in the mid-twenty-first century (**Figure 7**).

The Chesapeake Bay simulations focused on two decade-long periods: 1989–1998 and 2049–2058. A composite of the 1989–1998 period reveals typical warm-season carbonate chemistry distributions in the estuary (**Figure 7**), where an oxygen minimum zone exists in the deep midbay associated with a pH_T minimum. Between the 1990s and 2050s, temperature in the bay is projected to increase by approximately 1.5°C, relative sea level will rise approximately 0.5 m, and winter–spring river flows will increase by approximately 20%. Model projections forced by these changes suggest that DIC will increase by up to 80 μmol kg^{-1} and TA will increase by up to 60 μmol kg^{-1}, with the largest increase in the hypoxic bottom waters of the midbay. pH_T is projected to decrease

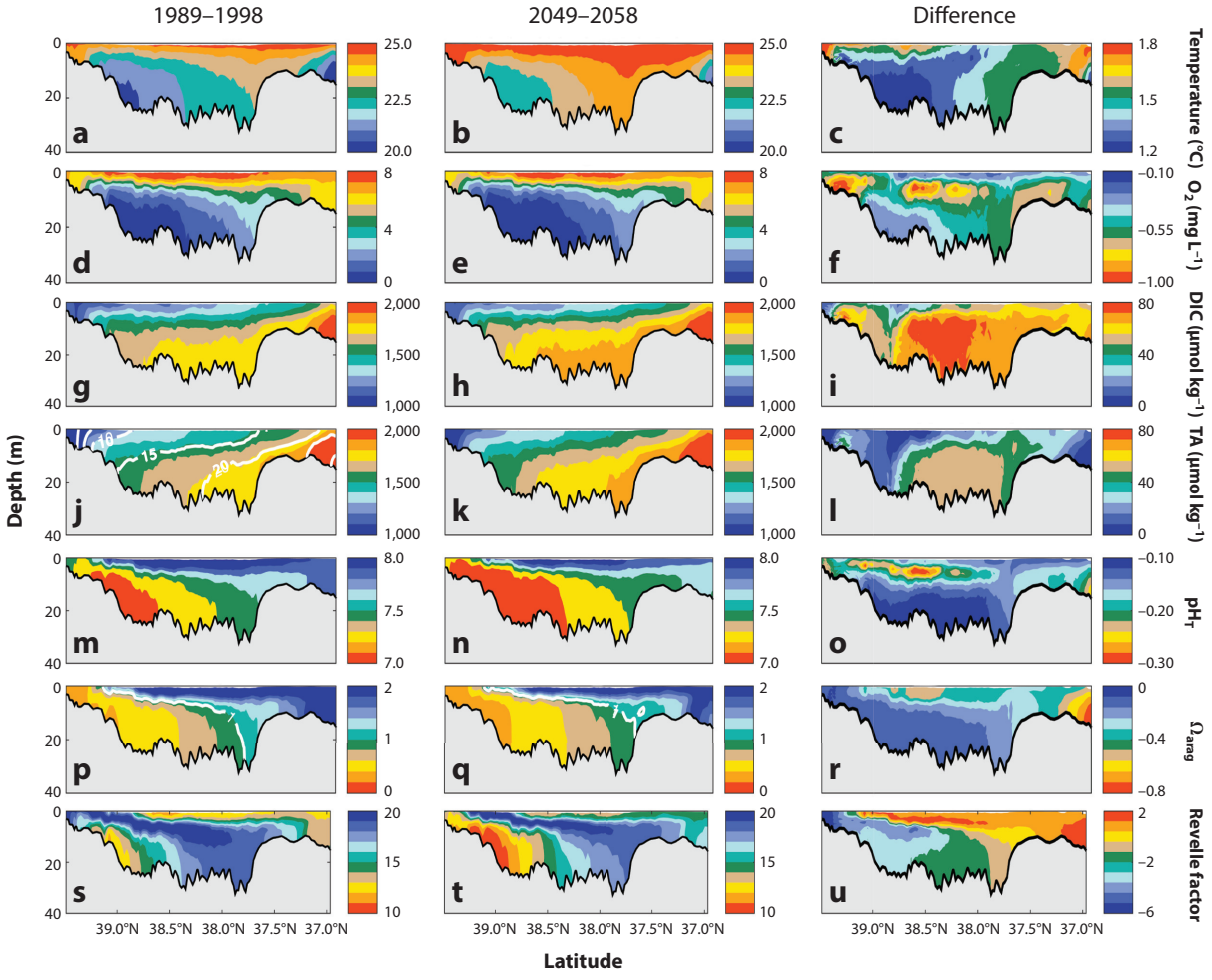

Figure 7

Model-predicted along-channel distributions of summer-averaged (*a–c*) temperature, (*d–f*) O_2, (*g–i*) DIC, (*j–l*) TA, (*m–o*) pH_T, (*p–r*) Ω_{arag}, and (*s–u*) Revelle factor in Chesapeake Bay, obtained from climate downscaling projections; the panels on the left show 1989–1998, the panels in the center show 2049–2058, and the panels on the right show the difference between the two. In the TA plot for 1989–1998 (panel *j*), salinity contour lines from low (*left*) to high (*right*) are marked with white lines at salinities of 1, 5, 10, 15, 20, 25, and 30. Regional climate models from NARCCAP (Mearns et al. 2013) were used to generate these plots. NARCCAP uses a dynamic climate downscaling approach by embedding fine-resolution (~50 km) regional climate models of North America into global climate models from CMIP3. NARCCAP simulations are available for a historical period (1971–2000) and the mid-twenty-first century (2041–2070) under the medium-high A2 greenhouse gas emissions scenario. RCM3-GFDL in the NARCCAP ensemble of regional climate models was used in the projection presented here. Abbreviations: CMIP3, Coupled Model Intercomparison Project Phase 3; DIC, dissolved inorganic carbon; GFDL, Geophysical Fluid Dynamics Laboratory; NARCCAP, North American Regional Climate Change Assessment Program; RCM3, Regional Climate Model Version 3; TA, total alkalinity.

by 0.1–0.3 (to as low as 7.1) over the 60-year period, with larger reductions at mid-depths (5–10 m) in the upper and middle parts of the estuary. Oxygen is projected to decrease by 0.2–1.0 mg L^{-1} (or 6–31 μmol kg^{-1}), with larger reductions in subsurface waters (5–10 m) and smaller reductions in hypoxic bottom waters. Ω_{arag} decreases throughout the bay, with a maximum decrease of 0.4 (to as low as 0.2) over the 60-year period. The aragonite undersaturated water, which occupies the

THE DIEL RANGE AND SEASONALITY OF ESTUARINE WATER PROPERTIES

In addition to the projected changes in mean properties, the ranges in pCO_2 and hydrogen ion concentration are expected to increase in the future, resulting in more extreme variations in weakly buffered estuarine waters (Baumann & Smith 2018, Feely et al. 2018). For example, elevated CO_2 was linked to elevated diel pH ranges in Chesapeake Bay (Shen et al. 2019a), while tide, temperature, and productivity also control diel pCO_2 (Dai et al. 2009). In productive habitats with submerged macrophytes, diel pH ranges can approach 1 pH unit (Pacella et al. 2018, Su et al. 2020a), suggesting additional alterations of diel cycles due to changes in macrophyte and phytoplankton productivity. Seasonal extremes are also projected to increase in the Salish Sea (Evans et al. 2019), where episodic summer wind mixing should drive higher-pCO_2 and lower-pH conditions, while winter levels will become more extreme in waters with a high DIC/TA ratio. In Chesapeake Bay, early-summer pH minima (pH < 7.5) would be muted if eutrophication is abated but enhanced if warming elevates respiration rates. Alterations of seasonal biogeochemical cycles are already underway (Testa et al. 2018), and the implications for short-term CO_2 system variability and the resulting biological response demand substantial research.

upper bay and lower depths of the midbay, expands farther seaward and toward the surface under future climate conditions. Finally, it is interesting to note that as anthropogenic CO_2 increases, the Revelle factor will increase (meaning that buffering weakens and pH sensitivity increases) in the high-salinity mid-lower bay, where $[CO_3^{2-}] > [CO_2]$, but decrease in the low-salinity upper bay, where $[CO_3^{2-}] < [CO_2]$. These results, which are based on more realistic estuarine settings, are consistent with predictions based on first principles as illustrated in **Figures 2** and **3**.

In summary, a warmer, wetter, high-CO_2 future in Chesapeake Bay is projected to include enhanced acidification, but unknown future changes in river chemistry, nutrient loading rates, and biological communities may alter this pathway. In addition to the projected changes in mean distributions of carbonate system properties, the diel range and seasonality would also increase under future climate conditions (see the sidebar titled The Diel Range and Seasonality of Estuarine Water Properties).

4.1.3. Ocean acidification impacts on economically important calcifiers across life stages of Chesapeake Bay calcifiers. Present-day summer pH_T and Ω_{arag} values in Chesapeake Bay surface waters are not detrimental for the larval stages of the eastern oysters or hard clams (Miller et al. 2009, Talmage & Gobler 2009). While the decline of future pH_T does not project surface exposure below the larval lethal threshold, it can compromise physiological processes related to growth, calcification, and lipid content and result in developmental delays and increased dissolution (Talmage & Gobler 2009). Negative juvenile responses occur at a lower pH_T and Ω_{arag} compared with the larval stage, where juvenile clams and eastern oysters inhabiting subsurface sediment habitats (>10 cm) exhibit calcification and growth decline at a pH_T of 7.5 or Ω_{arag} of 0.6 (Beniash et al. 2010, Green et al. 2009). Summer subsurface pH_T and Ω_{arag} within midbay bottom waters and smaller inlets within Chesapeake Bay are currently below these thresholds. This can trigger negative biological responses and increased energetic costs for organisms living outside the deepwater acidified regions if subsurface waters are upwelled to shallow shoals along the main stem bay or to shallow sub-estuarine waters that calcifiers currently occupy (**Figure 4**). Modeled future scenarios in Chesapeake Bay anticipate increased biological risks associated with a substantial expansion in the spatial extent of waters with low pH_T and Ω_{arag}, covering more than two-thirds of the entire subsurface basin (**Figure 7**). These simulations thus predict increased juvenile mortality, but not in the adult stages of clams and oysters, which are generally more resilient.

The impact on adults will be through the sublethal responses to oxidative stress and reduced calcification related to low pH_T (7.4–7.5) (Tomanek et al. 2011, Waldbusser et al. 2011) and increased dissolution at an Ω_{arag} of 0.7 (Ries et al. 2009). Such conditions are currently present on a regionally limited basis and will expand in the future but will likely not induce rapid population-level effects by midcentury. For other shell-forming organisms (e.g., blue crabs), the impacts of OA on some physiological processes may be outweighed by other factors that are expected to change in the future (e.g., warming; Glandon & Miller 2017), suggesting interactions between OA and other stressors.

4.2. The Salish Sea

The Salish Sea is an example of a glacially carved inland sea that has a large cumulative freshwater input that varies spatially over the region. It is representative of a comprehensive system of deep basins with a strong oceanic upwelling component.

4.2.1. Estuarine physics and carbonate chemistry. The Salish Sea is a fjord-type, semienclosed large estuarine system located in the Pacific Northwest. It is connected to the Pacific Ocean at its western end by the Strait of Juan de Fuca and at its northern end through Johnstone Strait, and comprises three main basins: Puget Sound, the central Strait of Georgia, and the northern Strait of Georgia. The vast majority of the water entering the Salish Sea is from the inflow of oceanic waters with salinities ranging from approximately 31 to 33.5 that are entrained in subsurface flows through the Strait of Juan de Fuca and then transported south into Puget Sound and north into the Strait of Georgia (Cannon et al. 1990, Feely et al. 2010, Masson 2006, Moore et al. 2008, Pawlowicz et al. 2007). Deepwater inflow to the Salish Sea tends to be colder and saltier in the late summer because of upwelling of cold, CO_2-enriched, oxygen-depleted water along the coast.

Puget Sound encompasses the region south of Admiralty Reach, including Hood Canal, Whidbey Basin, the main basin, and South Sound (**Figure 8**). This inflow undergoes mixing with the outflowing low-salinity, river-derived surface water (0–20 m) at Admiralty Reach and within the Strait of Juan de Fuca. In this analysis, we focused on the portion of Puget Sound comprising Admiralty Reach, the main basin, and South Sound. The mean residence time of the waters in the deep Puget Sound basins is approximately two to four months (Moore et al. 2008, Sutherland et al. 2011), which differs from the one- to three-year estimate for deepwater residence time in the deeper Strait of Georgia (Pawlowicz et al. 2007). Conditions vary with depth, over time, and spatially (Feely et al. 2010). In summer, strong vertical gradients of salinity, DIC, pH_T, and Ω_{arag} form in the upper 8 m of the main basin and South Sound, where freshwater input and primary production play a significant role in increasing pH_T and Ω_{arag} and decreasing DIC. Outflowing surface waters have pH_T values ranging from approximately 7.8 to 8.3 and Ω_{arag} values ranging from approximately 1.0 to 2.0. In deeper waters below 25 m, pH_T values range from approximately 7.7 to 7.9, and Ω_{arag} values range from approximately 0.8 to 1.3. In winter, stratification decreases substantially, and pH_T values drop to below 7.8, while Ω_{arag} values range from 0.7 to 0.9 (Feely et al. 2010). Similar patterns are observed to the north in the Strait of Georgia (Ianson et al. 2016, Moore-Maley et al. 2016), although summer stratification there is at times disrupted by strong southward, along-channel winds that drive high pCO_2, low pH, and undersaturated Ω_{arag} at the surface (Evans et al. 2019). Present-day (2008–2018) anthropogenic CO_2 concentrations in surface and subsurface waters of the Salish Sea range from 13 to 49 $\mu mol\ kg^{-1}$, with an uncertainty of approximately 10% based on the ΔpCO_2 and ΔTCO_2 methods, varying by basin and habitat (Evans et al. 2019, Feely et al. 2010, Pacella et al. 2018).

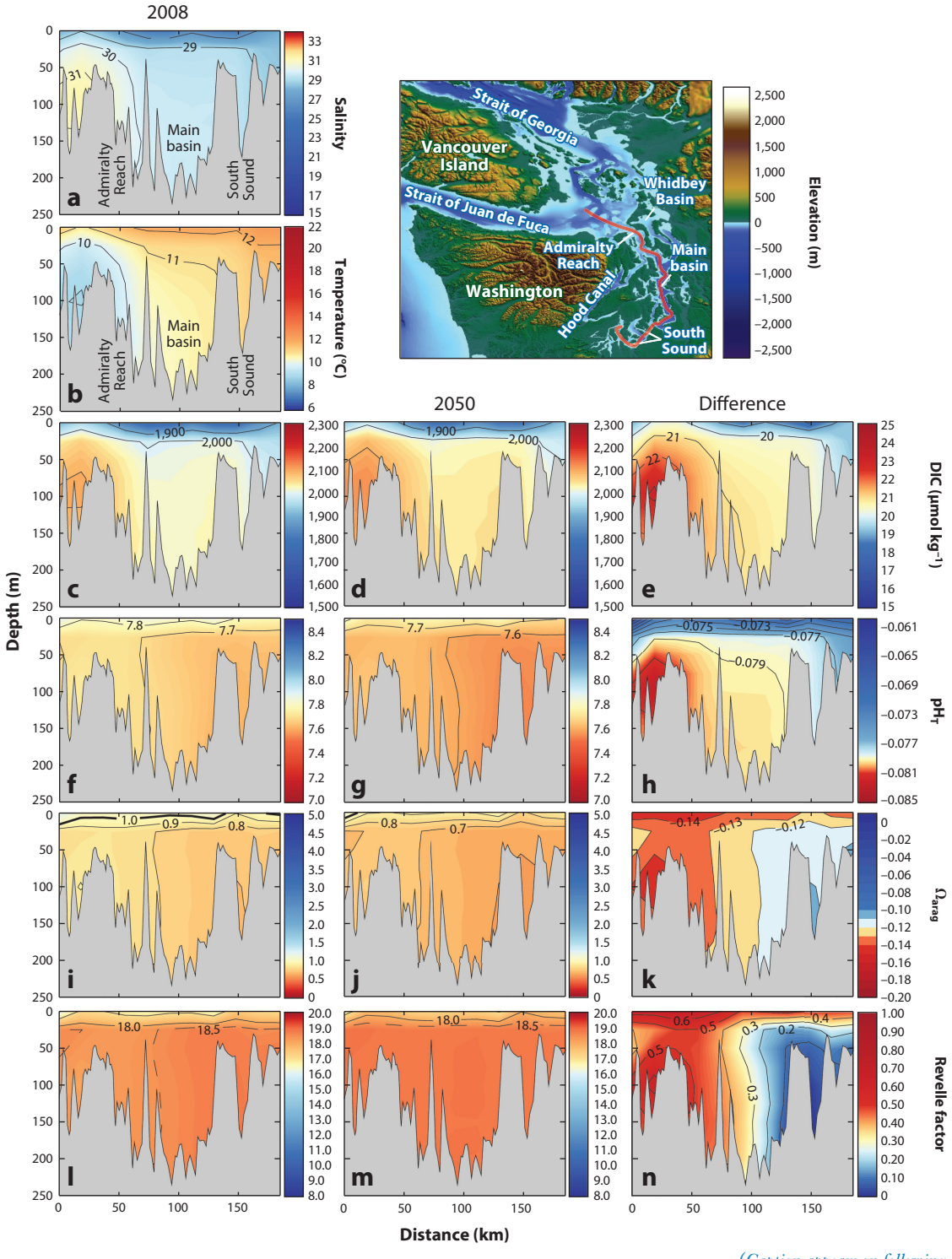

(*Caption appears on following page*)

Figure 8 (*Figure appears on preceding page*)

Distributions of 2008 mean annual (*a*) salinity, (*b*) temperature, (*c*) DIC, (*f*) pH_T, (*i*) Ω_{arag}, and (*l*) Revelle factor in Puget Sound waters (*top right inset*), based on the Salish Sea Model; distributions of 2050 mean annual (*d*) DIC, (*g*) pH_T, (*j*) Ω_{arag}, and (*m*) Revelle factor; and the difference between the 2050 and 2008 distributions based on the model for mean annual (*e*) DIC, (*h*) pH_T, (*k*) Ω_{arag}, and (*n*) Revelle factor. The Salish Sea Model is an application of the unstructured grid Finite-Volume Community Ocean Model, with the addition of a biogeochemical component of the Integrated Compartment Model (Chen et al. 2003, Khangaonkar et al. 2012, Kim & Khangaonkar 2012) that includes two-layer sediment and the carbonate system variables (TA and DIC) in the water column. Abbreviations: DIC, dissolved inorganic carbon; TA, total alkalinity.

4.2.2. Projections into the future. The Salish Sea Model provides average conditions for salinity, temperature, DIC, pH, Ω_{arag}, and Revelle factor for model year 2008; projections of mean annual DIC, pH, Ω_{arag}, and Revelle factor in 2050; and the difference between the two (**Figure 8**). Results from this model indicate that the predominant drivers of lower pH and Ω_{arag} in Puget Sound waters include anthropogenic DIC from local air–sea exchange, input from the coast in subsurface waters, and input from subsurface remineralization of organic matter, combined with low wind mixing and stratification in most areas (Bianucci et al. 2018, Pelletier et al. 2018). The largest gradients of DIC, pH, and Ω_{arag} occur in the upper 5–25 m of the water column, where vertical gradients and seasonal variability are highest. Below approximately 25 m, horizontal gradients predominate. The most significant anthropogenic drivers include global atmospheric CO_2 increase and local eutrophication, which are responsible for the most significant contributions to changing coastal and estuarine acidification conditions in the region (Feely et al. 2010, 2012a; Pacella et al. 2018; Pelletier et al. 2018; Evans et al. 2019).

Since biological processes take up carbon in the spring, summer, and early fall months and release it at depth via respiration processes, there are strong vertical gradients in DIC, pH_T, and Ω_{arag} throughout the region. The Salish Sea Model output, based on the Representative Concentration Pathway (RCP) 8.5 CO_2 emission scenario, indicates that the largest DIC increases, of up to approximately 25 $\mu mol\ kg^{-1}$ between 2008 and 2050, are associated with inflowing coastal waters that contain the highest amounts of anthropogenic CO_2 (Evans et al. 2019, Feely et al. 2016). This water flows over the sill at Admiralty Reach and mixes into the deeper waters of the main basin, Hood Canal, and South Sound, eventually mixing upward to the surface during winter overturn. Similarly, the largest decreases in pH_T (as much as 0.08) and Ω_{arag} (as much as 0.15) occur in the inflowing subsurface waters into the main basin from the Strait of Juan de Fuca. Significant changes in pH_T also occur in surface and subsurface waters throughout the South Sound region, where buffer capacity is low (high Revelle factor) and eutrophication is high. The smaller changes in anthropogenic DIC in the Salish Sea relative to the coast are due to the dilution effect of mixing of riverine water with the older coastal subsurface water. These changes in water column conditions are enough to drop below several critical thresholds for economically and ecologically important calcifying species in the region (Bednaršek et al. 2018).

4.2.3. Ocean acidification impact considerations across life stages of Puget Sound calcifiers. The model output indicates that, in 2008, the subsurface waters of the main basin of Puget Sound had pH_T values of approximately 7.7–7.9 and an Ω_{arag} of approximately 1 (**Figure 8**; see also Feely et al. 2010), which represent less-than-optimal exposure for a variety of marine calcifiers. Such exposure can trigger a myriad of physiological and energetic compromises for larval stages of a variety of ecologically and economically important species, including Pacific and Olympia oysters, California mussels, pteropods, Dungeness crab, and the endangered northern abalone. Negative responses, as observed under the experimental conditions below a pH_T of 7.8–8 and Ω_{arag} of 1.4–2, are linked to increased dissolution, impaired larval development and survival, and reduced calcification (Bednaršek et al. 2019, 2020a; Crim et al. 2011; Waldbusser et al. 2015b).

With respect to juveniles, reduced shell growth and mortality of Olympia oysters can occur at a pH_T of 7.8 if their larval stages were exposed to low pH_T (Hettinger et al. 2012). This has been confirmed by field biological observations of different magnitudes of pteropod shell dissolution across the entire Puget Sound (Bednaršek et al. 2020b).

With respect to future biological exposure, the largest pH_T change will occur in subsurface habitats below 5 m, while Ω_{arag} decrease is projected to occur throughout surface and subsurface waters (**Figure 8**). Such future conditions will make physiological processes across all life stages of calcifiers more challenging, potentially even lethal. One such example includes the economically important Dungeness crab, with increased larval mortality related to exposure below a pH_T of 7.5 (Miller et al. 2016).

Compared with Chesapeake Bay, the main basin of Puget Sound is relatively uniform in its vertical distributions of the carbonate species and pH_T (**Figures 7** and **8**), indicating that organisms on an annual basis experience less variable exposure to biologically relevant carbonate chemistry parameters (with pH_T changes of approximately 0.1–0.2 and Ω_{arag} changes of 0.1). This suggests that marine calcifiers in the main basin of Puget Sound may not be as naturally adapted to variation in carbonate chemistry as those in Chesapeake Bay.

4.3. Prince William Sound

The final example we consider is Prince William Sound, located in the northern Gulf of Alaska. This deep, subarctic fjord complex is representative of similar regions that receive significant freshwater input, including large contributions of cold glacial meltwater, and with seasonally modified connectivity to the open continental shelf.

4.3.1. Estuarine physics and carbonate chemistry. Prince William Sound (**Figure 9**) is a large, subarctic, estuarine fjord complex on the south-central coast of Alaska (Halverson et al. 2013, Musgrave et al. 2013) with two openings to the North Pacific: Hinchinbrook Entrance and Montague Strait. Surface water from the westward-flowing Alaska Coastal Current on the adjacent continental shelf typically enters the sound through Hinchinbrook Entrance and then exits through Montague Strait. This flow-through circulation pattern is enhanced during winter, when winds drive shoreward surface flow over the continental shelf and increase Alaska Coastal Current transport (Halverson et al. 2013, Stabeno et al. 2004, Weingartner et al. 2005), and reduced during summer. Prince William Sound is part of the North American region experiencing the greatest glacial mass loss globally, with glacial melt as a substantial contributor to the total regional freshwater discharge (Neal et al. 2010, Weingartner et al. 2005).

Seawater dissolved oxygen, temperature, salinity, DIC, TA, and macronutrients were sampled through the water column at several stations in Prince William Sound every May and September from 2009 to 2012 (Evans et al. 2014). In particular, data from one station on the northwestern side (PWS2 in **Figure 9*a***) demonstrate that the overall patterns in the sound are as follows: (*a*) Deepwater temperature, salinity, DIC, and TA values differed little between May and September, presumably due to the short residence time of water within the sound; (*b*) the spring phytoplankton bloom during April and May resulted in a large near-surface vertical gradient in DIC without corresponding gradients in temperature, salinity, and TA; and (*c*) freshening of the upper 30 m in autumn corresponded with large gradients in DIC and TA and the occurrence of undersaturation for aragonite despite a seasonal warming from 6°C to near 12°C. Water below 500 m maintained stable temperature, salinity, DIC, and TA levels, with a corresponding DIC/TA ratio of 0.97. The DIC/TA ratio near the surface in spring decreased to nearly 0.9 owing to CO_2 drawdown, which drove the highest observed Ω_{arag}, of nearly 2.8. Glacial melt input to the sound in

Figure 9

(*a*) The fjord complex of Prince William Sound, which has a maximum depth near 800 m, inflow through Hinchinbrook Entrance, and outflow through Montague Strait. (*b–i*) Data from hydrographic station PWS2 (shown in panel *a*), sampled every May and September from 2009 to 2012 (Evans et al. 2014). Panels *b* and *c* are depth profiles of the mean and standard deviation (*shaded area*) for spring pH_T and Ω_{arag}, respectively, and panels *d* and *e* are the differences between 2050 and mean 2008–2012 values; panels *f–i* are the same for the fall season. Uncertainty due to environmental variability was expressed in terms of the standard deviation of measurements from each depth and season. Uncertainty in the resulting anthropogenic CO_2 estimates is near 10% (Sabine et al. 2002). The bathymetry in panel *a* is from the Prince William Sound, Alaska 8/3 Arc-second MHHW Coastal Digital Elevation Model provided (Natl. Geophys. Data Cent. 2009).

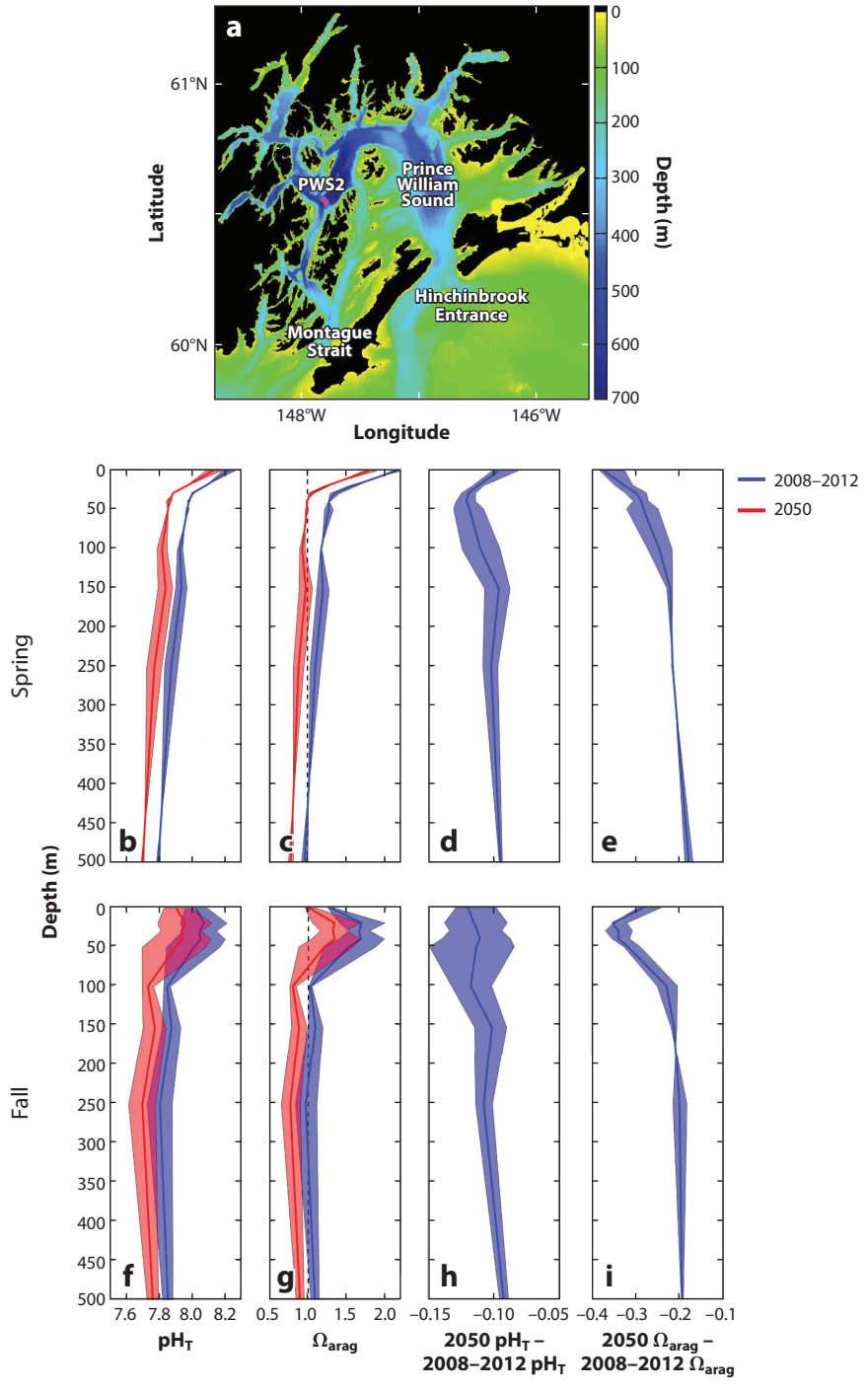

the autumn resulted in interesting CO_2 chemistry patterns, where DIC and TA were diluted to 1,237 μmol kg^{-1} and 1,285 μmol kg^{-1}, respectively, in the freshest (salinity of 18.7) and coldest (6.1°C) observed meltwater, which resulted in low [CO_3^{2-}] and Ω_{arag} near 0.6, a pH_T of 8.0, and surface pCO_2 of 286 μatm. The observed melt plumes were also corrosive for calcite. Having very low Ω_{arag}, relatively high pH_T, and low pCO_2 simultaneously is a unique characteristic of higher-latitude estuaries that receive cold fresh water, which sets them apart from estuarine systems in lower latitudes, such as Chesapeake Bay and the Mississippi River plume region. The condition of pCO_2 undersaturation in the melt plume should lead to uptake of CO_2 from the atmosphere, thereby maintaining low-Ω_{arag} conditions as plume water exits the estuary.

4.3.2. Future changes in anthropogenic CO_2 accumulation. We evaluated the influence of anthropogenic CO_2 addition between 2012 and 2050 on pH_T and Ω_{arag} conditions within Prince William Sound using spring (May) and autumn (September) mean observations collected at station PWS2 (**Figure 9*a***) with the ΔTCO_2 approach for estimating anthropogenic CO_2 described previously (Evans et al. 2019, Sabine et al. 2002, Takeshita et al. 2015), which was corrected for water mass age (i.e., last contact with the atmosphere) using the mean profile of apparent oxygen utilization divided by oxygen utilization rate for North Pacific water (Feely et al. 2004). The atmospheric CO_2 content used in the ΔTCO_2 approach to estimate seawater DIC concentrations in 2050 was from the high-emissions RCP 8.5 scenario (Riahi et al. 2011). Anthropogenic CO_2 content accrued over the 2012–2050 period was taken to be the difference in DIC between 2012 and 2050 for each season, and uncertainty in these estimates is near 10% (Sabine et al. 2002). Below 200 m, anthropogenic CO_2 content was not appreciably different between May and September, with mean values ranging from 25 to 27 μmol kg^{-1}. Nearer to the surface, these values were higher and more variable due to water having recent contact with the atmosphere and varying Revelle factors. Maximum mean values are near 39 μmol kg^{-1}, with the lowest instantaneous levels associated with water with a high DIC/TA ratio. This value of anthropogenic CO_2 implies an increase rate of approximately 1 μmol kg^{-1} y^{-1}, which agrees with increase rate estimates for Gulf of Alaska surface water (Carter et al. 2019).

The effects of this anthropogenic CO_2 addition on pH_T and Ω_{arag} are shown in **Figure 9**, with the degree of pH_T and Ω_{arag} decrease varying with depth and season. During spring, the largest change in pH_T is estimated to occur below the surface layer, at between 50 and 150 m, whereas Ω_{arag} will likely change most near the surface. During autumn, the largest changes in both parameters are estimated to be in the upper 200 m, though with large variability in the degree of change depending on the state of the DIC/TA ratio. Importantly, during both spring and autumn, the water column below 100 m is anticipated to become corrosive to aragonite, representing an almost 85% reduction in noncorrosive habitat for calcifiers utilizing this biomineral. This projected change below the surface layer has yet to be considered by assessments of regional vulnerability and would have direct and indirect impacts for several locally important fisheries (Mathis et al. 2015).

4.3.3. Ocean acidification–related biological impacts in Prince William Sound. In comparison with Chesapeake Bay and the Salish Sea, the depth range and seasonal pH and Ω_{arag} conditions in Prince William Sound are higher, which may suggest a more favorable habitat overall for a variety of ecologically and economically important estuarine calcifying species. Present-day conditions in the sound might already impact some of these species, including selected crustacean, pteropod, and echinoderm species. Under projected 2050 conditions, this could lead to heightened vulnerability in some species.

Among the economically and ecologically significant crustaceans that might be negatively impacted under present-day pH conditions are juvenile stages of red king crab and Tanner crab. Their life histories and vertical distributions to depths of 200 m and 440 m, respectively, expose them to low-pH conditions (down to $pH_T \sim 7.8$) that can lead to slower growth and increased mortality for both species and retarded development for juvenile red king crabs (Long et al. 2013a,b). Predicted pH conditions by 2050 ($pH_T \sim 7.7$) may be detrimental to the fitness and survival of the larval stages of both species, especially when female adults experience prolonged exposure.

Pteropods in the sound represent a substantial dietary resource for a variety of juvenile fish species, especially in the autumn (Auburn & Ignell 2000, Doubleday & Hopcroft 2015). Current Ω_{arag} conditions ($\Omega_{arag} \sim 1$) in the upper 100 m may induce severe shell dissolution (Bednaršek et al. 2014). Decreasing Ω_{arag} conditions both at the surface and below 50 m will truncate suitable habitat for this organisms and lead to potentially high levels of shell dissolution, as well as other physiological and reproductive impairments that may lead to increases in mortality, decreased calcification, and population-level effects (Bednaršek et al. 2014, 2017, 2019).

Present-day low-pH exposure might also include negative impacts on the red sea urchin, with decreased fertilization efficiency and reproductive success at pH_T of 7.8 (Reuter et al. 2011). Such conditions are found in the autumn in the upper 120 m of their vertical habitat (Bernard 1977, Kato & Schroeter 1985) and may decrease further in the future. The 2050 pH_T prediction may also lead to heightened vulnerability for the larvae of Baltic clam (Jansson et al. 2016), as they require prolonged settlement time at lower-pH_T conditions.

5. SUMMARY AND FUTURE CONSIDERATIONS

Large estuaries and bays are uniquely sensitive to OA because they are a central connection point for exchange and mixing of river water with seawater, generally producing large vertical and horizontal gradients, which vary seasonally. With inputs of poorly buffered fresh waters and long water residence times, these estuaries are particularly vulnerable, in terms of rapid decreases in pH and Ω_{arag}, to increased CO_2 loading due to air–sea exchange of anthropogenic CO_2, enhanced respiration due to high nutrient input and eutrophication, and the addition and subsequent degradation of dissolved and particulate organic matter. In particular, in estuaries with freshwater input of low-to-intermediate TA values, the combination of an increasing acid–base sensitivity factor or a decreasing buffer factor (with decreasing salinity) and a still-strong oceanic OA signal can generate a minimum buffer zone and thus a maximum estuarine acidification zone. The increase in pCO_2 and decrease in pH in many large estuaries are expected to accelerate over time, with the greatest changes occurring in regions where the sensitivity increases and the buffer capacity decreases the most. Depending on local warming rate, the decrease in Ω_{arag} may slow down in the future (Feely et al. 2018).

The changes in chemistry either already have imposed physiological and energetic compromises on some calcifiers in large estuaries or will in the future, when potentially lethal thresholds will be crossed. Increased chemical and biological monitoring and improved understanding and modeling of the local biogeochemical processes will make it easier to predict what impact prolonged exposure will have on multiple carryover effects from larval to adult stages, likely exacerbating the vulnerability of calcifiers. This is of enormous importance in the context of commercial shellfish and aquaculture, where sustainability may be threatened unless it is closely linked to monitoring of suitable habitats in the region. Indeed, experimental and field chemical and biological studies should primarily strive to address and understand the effects of the drivers that shape the

natural variability of estuarine systems across different temporal and spatial scales, co-occurring with the added drivers of thermal and hypoxic stress.

It is still rather difficult to fully explain and predict how individual carbonate species respond to higher CO_2 levels and changing physical and biogeochemical conditions in low-salinity estuarine waters located in different climate zones. The challenges include the need for a set of more precisely determined thermodynamic constants with known uncertainties in low-salinity waters, a clearly defined pH scale bridging fresh water and seawater, and an accurate and easy-to-use analytical method and set of standards for determining estuarine pH. The challenges also include an urgent need to build a better chemical model for aquatic acid–base chemistry, in particular one that shows how organic acid–base reactions contribute to TA in estuarine waters with high levels of dissolved organic carbon. The findings summarized here underscore the critical need for attention to the role of natural and anthropogenic acidification in estuaries. The findings that large estuaries are particularly sensitive to acidification effects because of their connection to fresh waters, that such estuaries have high spatial and seasonal complexity, and that calcifiers are already experiencing effects (and are projected for more) serve as a strong impetus for increased study, particularly when coupled with the ecological and economic importance and societal reliance on resources from estuaries worldwide (Barbier et al. 2011, Thrush et al. 2014). Furthermore, the recognition that we face multiple challenges, from accurate measurement to better modeling, should be a unifying call to the scientific community. We need more coordinated collaborative research on estuarine physical, chemical, and biological processes with contrasting timescales—from (*a*) rapid chemical equilibrium, to (*b*) physical mixing on hourly to monthly timescales (tidal, circulation, upwelling, etc.), to (*c*) weekly and seasonally changing biological production and respiration and $CaCO_3$ formation, dissolution, and sensitivity to OA conditions. Progress on these research topics is critical for a better understanding and prediction of the chemical and biological responses to a warmer and higher-CO_2 world. A wider understanding and appreciation of this information, among not only scientists but also managers and policy makers, will enable better-informed actions.

DISCLOSURE STATEMENT

The authors are not aware of any affiliations, memberships, funding, or financial holdings that might be perceived as affecting the objectivity of this review.

AUTHOR CONTRIBUTIONS

W.-J.C. and R.A.F. planned the article. All authors contributed to Sections 1 and 5. W.-J.C. wrote Sections 2 and 3 and created **Figures 2–6**. Y.-Y.X. contributed to Sections 2 and 3. J.M.T., M.L., and W.-J.C. wrote Section 4.1. M.L. created **Figure 7**. R.A.F., W.E., J.A.N., S.R.A., A.A., G.P., and D.J.G. wrote Section 4.2 and created **Figure 8**. N.B. wrote Sections 4.1.3, 4.2.3, and 4.3.3. W.E. wrote Section 4.3 and created **Figure 9**.

ACKNOWLEDGMENTS

This work was supported by the National Oceanic and Atmospheric Administration (NOAA) (grants OAPFY2018.03.PMEL.003, NA15NOS4780184, NA15NOS4780190, and NA18NOS4780179) and the National Science Foundation's Chemical Oceanography Program (OCE-1559279). We specifically thank Libby Jewett, Dwight Gledhill, and Erica Ombres of the NOAA Ocean Acidification Program and Elizabeth Turner of the NOAA National Centers for

Coastal Ocean Science for their support. The University of Washington Ocean Acidification Center and the Washington State Department of Ecology provided support for the 2008 Puget Sound data and the Salish Sea Model. W.-J.C. thanks Professor J. Gan and the Department of Mathematics at the Hong Kong University of Science and Technology for hosting his sabbatical leave, during which a portion of this article was written. **Figure 1** was constructed using the University of Maryland Center for Environmental Science (UMCES) Integration and Application Network symbol library. This is contribution number 5092 from the NOAA Pacific Marine Environmental Laboratory, UMCES contribution number 5867, and Ref. No. [UMCES] CBL 2020-135.

LITERATURE CITED

Abril G, Etcheber H, Delille B, Frankignoulle M, Borges AV. 2003. Carbonate dissolution in the turbid and eutrophic Loire estuary. *Mar. Ecol. Prog. Ser.* 259:129–38

Adelsman H, Binder LW, eds. 2012. *Ocean acidification: from knowledge to action*. Rep., Wash. State Dep. Ecol., Olympia

Albright R, Takeshita Y, Koweek DA, Ninokawa A, Wolfe K, et al. 2018. Carbon dioxide addition to coral reef waters suppresses net community calcification. *Nature* 555:516–19

Álvarez M, Sanleón-Bartolomé H, Tanhua T, Mintrop L, Luchetta A, et al. 2014. The CO_2 system in the Mediterranean Sea: a basin wide perspective. *Ocean Sci.* 10:69–92

Auburn ME, Ignell SE. 2000. Food habits of juvenile salmon in the Gulf of Alaska July–August 1996. *North Pac. Anadramous Fish Comm. Bull.* 2:89–97

Barbier EB, Hacker SD, Kennedy C, Koch EW, Stier AC, Silliman BR. 2011. The value of estuarine and coastal ecosystem services. *Ecol. Monogr.* 81:169–93

Barton A, Waldbusser GG, Feely RA, Weisberg SB, Newton JA, et al. 2015. Impacts of coastal acidification on the Pacific Northwest shellfish industry and adaptation strategies implemented in response. *Oceanography* 28(2):146–159

Bates NR, Astor Y, Church M, Currie K, Dore J, et al. 2014. A time-series view of changing ocean chemistry due to ocean uptake of anthropogenic CO_2 and ocean acidification. *Oceanography* 27(1):126–41

Bates NR, Best MHP, Neely K, Garley R, Dickson AG, Johnson RJ. 2012. Detecting anthropogenic carbon dioxide uptake and ocean acidification in the North Atlantic Ocean. *Biogeosciences* 9:2509–22

Bates RG. 1973. *Determination of pH: Theory and Practice*. New York: Wiley & Sons

Baucke FG. 2002. New IUPAC recommendations on the measurement of pH – background and essentials. *Anal. Bioanal. Chem.* 374:772–77

Baumann H, Smith EM. 2018. Quantifying metabolically driven pH and oxygen fluctuations in US nearshore habitats at diel to interannual time scales. *Estuaries Coasts* 41:1102–17

Bednaršek N, Feely RA, Beck MW, Alin SR, Siedlecki SA, et al. 2020a. Exoskeleton dissolution with mechanoreceptor damage in larval Dungeness crab related to severity of present-day ocean acidification vertical gradients. *Sci. Total Environ.* 716:136610

Bednaršek N, Feely RA, Beck MW, Glippa O, Kanerva M, Engström-Öst J. 2018. El Niño-related thermal stress coupled with upwelling-related ocean acidification negatively impacts cellular to population-level responses in pteropods along the California Current System with implications for increased bioenergetic costs. *Front. Mar. Sci.* 5:486

Bednaršek N, Feely RA, Howes EL, Hunt BP V, Kessouri F, et al. 2019. Systematic review and meta-analysis toward synthesis of thresholds of ocean acidification impacts on calcifying pteropods and interactions with warming. *Front. Mar. Sci.* 6:227

Bednaršek N, Feely RA, Reum JCP, Peterson B, Menkel J, et al. 2014. *Limacina helicina* shell dissolution as an indicator of declining habitat suitability owing to ocean acidification in the California Current Ecosystem. *Proc. R. Soc. B* 281:20140123

Bednaršek N, Feely RA, Tolimieri N, Hermann AJ, Siedlecki SA, et al. 2017. Exposure history determines pteropod vulnerability to ocean acidification along the US West Coast. *Sci. Rep.* 7:4526

Bednaršek N, Newton JA, Beck MW, Alin SR, Feely RA, et al. 2020b. Severe biological effects under present-day estuarine acidification in the seasonally variable Salish Sea. *Sci. Total Environ.* In press. **https://doi.org/10.1016/j.scitotenv.2020.142689**

Beniash E, Ivanina A, Lieb NS, Kurochkin I, Sokolova IM. 2010. Elevated level of carbon dioxide affects metabolism and shell formation in oysters *Crassostrea virginica* (Gmelin). *Mar. Ecol. Prog. Ser.* 419:95–108

Bernard FR. 1977. Fishery and reproductive cycle of the red sea urchin, *Strongylocentrotus franciscanus*, in British Columbia. *J. Fish. Board Can.* 34:604–10

Bianucci L, Long W, Khangaonkar T, Pelletier G, Ahmed A, Mohamedali T. 2018. Sensitivity of the regional ocean acidification and the carbonate system in Salish Sea to ocean and freshwater inputs. *Elem. Sci. Anthr.* 6:22

Borges AV, Abril G. 2011. Carbon dioxide and methane dynamics in estuaries. In *Treatise on Estuarine and Coastal Science*, Vol. 5, ed. E Wolanski, D McLusky, pp. 119–61. Waltham, MA: Academic

Borges AV, Gypens N. 2010. Carbonate chemistry in the coastal zone responds more strongly to eutrophication than ocean acidification. *Limnol. Oceanogr.* 55:346–53

Boudreau BP, Canfield DE. 1993. A comparison of closed-system and open-system models for porewater pH and calcite-saturation state. *Geochim. Cosmochim. Acta.* 57:317–34

Brewer PG. 2009. A changing ocean seen with clarity. *PNAS* 106:12213–14

Brodeur JR, Chen B, Su J, Xu Y, Hussain N, et al. 2019. Chesapeake Bay inorganic carbon: spatial distribution and seasonal variability. *Front. Mar. Sci.* 6:99

Buck RP, Rondinini S, Covington AK, Baucke FGK, Brett CMA, et al. 2002. Measurement of pH. Definition, standards, and procedures (IUPAC recommendations 2002). *Pure Appl. Chem.* 74:2169–200

Cai W-J. 2011. Estuarine and coastal ocean carbon paradox: CO_2 sinks or sites of terrestrial carbon incineration? *Annu. Rev. Mar. Sci.* 3:123–45

Cai W-J, Chen F, Powell EN, Walker SE, Parsons-Hubbard KM, et al. 2006. Preferential dissolution of carbonate shells driven by petroleum seep activity in the Gulf of Mexico. *Earth Planet. Sci. Lett.* 248:227–43

Cai W-J, Guo X, Chen C-TA, Dai M, Zhang L, et al. 2008. A comparative overview of weathering intensity and HCO_3^- flux in the world's major rivers with emphasis on the Changjiang, Huanghe, Zhujiang (Pearl) and Mississippi Rivers. *Cont. Shelf Res.* 28:1538–49

Cai W-J, Hu X, Huang W-J, Jiang L-Q, Wang Y, et al. 2010a. Alkalinity distribution in the western North Atlantic Ocean margins. *J. Geophys. Res. Oceans* 115:1538–49

Cai W-J, Hu X, Huang W-J, Murrell MC, Lehrter JC, et al. 2011. Acidification of subsurface coastal waters enhanced by eutrophication. *Nat. Geosci.* 4:766–70

Cai W-J, Huang W-J, Luther GW, Pierrot D, Li M, et al. 2017. Redox reactions and weak buffering capacity lead to acidification in the Chesapeake Bay. *Nat. Commun.* 8:369

Cai W-J, Luther GW III, Cornwell JC, Giblin AE. 2010b. Carbon cycling and the coupling between proton and electron transfer reactions in aquatic sediments in Lake Champlain. *Aquat. Geochem.* 16:421–46

Cai W-J, Pomeroy LR, Moran MA, Wang YC. 1999. Oxygen and carbon dioxide mass balance for the estuarine-intertidal marsh complex of five rivers in the southeastern US. *Limnol. Oceanogr.* 44:639–49

Cai W-J, Reimers CE. 1993. The development of pH and pCO_2 microelectrodes for studying the carbonate chemistry of pore waters near the sediment-water interface. *Limnol. Oceanogr.* 38:1762–73

Cai W-J, Wang Y. 1998. The chemistry, fluxes, and sources of carbon dioxide in the estuarine waters of the Satilla and Altamaha Rivers, Georgia. *Limnol. Oceanogr.* 43:657–68

Cai W-J, Wang Y, Hodson RE. 1998. Acid-base properties of dissolved organic matter in the estuarine waters of Georgia, USA. *Geochim. Cosmochim. Acta.* 62:473–83

Cai W-J, Xu Y-Y, Feely RA, Wanninkhof R, Jönsson B, et al. 2020. Controls on surface water carbonate chemistry along North American ocean margins. *Nat. Commun.* 11:2691

Caldeira K, Wickett ME. 2003. Anthropogenic carbon and ocean pH. *Nature* 425:365

Canfield DE, Jorgensen BB, Fossing H, Glud R, Gundersen J, et al. 1993. Pathways of organic carbon oxidation in three continental margin sediments. *Mar. Geol.* 113:27–40

Cannon GA, Holbrook JR, Pashinski DJ. 1990. Variations in the onset of bottom-water intrusions over the entrance sill of a fjord. *Estuaries* 13:31–42

Carter BR, Feely RA, Wanninkhof R, Kouketsu S, Sonnerup RE, et al. 2019. Pacific anthropogenic carbon between 1991 and 2017. *Glob. Biogeochem. Cycles* 33:597–617

Carter HH, Pritchard DW. 1988. Oceanography of Chesapeake Bay. In *Hydrodynamics of Estuaries*, Vol. 2: *Estuarine Case Studies*, ed. B Kjerfve, pp. 1–16. Boca Raton, FL: CRC

Chan F, Boehm AB, Barth JA, Chornesky EA, Dickson AG, et al. 2016. *The West Coast Ocean Acidification and Hypoxia Science Panel: major findings, recommendations, and actions*. Rep., Calif. Ocean Sci. Trust, Oakland

Chen C, Liu H, Beardsley RC. 2003. An unstructured grid, finite-volume, three-dimensional, primitive equations ocean model: application to coastal ocean and estuaries. *J. Atmos. Ocean. Technol.* 20:159–86

Clayton TD, Byrne RH. 1993. Spectrophotometric seawater pH measurements: total hydrogen ion concentration scale calibration of *m*-cresol purple and at-sea results. *Deep-Sea Res. I* 40:2115–29

Crim R, Sunday J, Harley C. 2011. Elevated seawater CO_2 concentrations impair larval development and reduce larval survival in endangered northern abalone (*Haliotis kamtschatkana*). *J. Exp. Mar. Biol. Ecol.* 400:272–77

Dai M, Lu Z, Zhai W, Chen B, Cao Z, et al. 2009. Diurnal variations of surface seawater CO_2 in contrasting coastal environments. *Limnol. Oceanogr.* 54:735–45

Dickson AG. 1993. The measurement of sea water pH. *Mar. Chem.* 44:131–42

Dickson AG, Camões MF, Spitzer P, Fisicaro P, Stoica D, et al. 2016. Metrological challenges for measurements of key climatological observables. Part 3: seawater pH. *Metrologia* 53:R26

Doney SC, Busch DS, Cooley SR, Kroeker KJ. 2020. The impacts of ocean acidification on marine ecosystems and reliant human communities. *Annu. Rev. Environ. Resour.* 45:83–112

Doney SC, Fabry VJ, Feely RA, Kleypas JA. 2009. Ocean acidification: the other CO_2 problem. *Annu. Rev. Mar. Sci.* 1:69–92

Doubleday AJ, Hopcroft RR. 2015. Interannual patterns during spring and late summer of larvaceans and pteropods in the coastal Gulf of Alaska, and their relationship to pink salmon survival. *J. Plankton Res.* 37:134–50

Du J, Shen J. 2016. Water residence time in Chesapeake Bay for 1980–2012. *J. Mar. Syst.* 164:101–11

Egleston ES, Sabine CL, Morel FMM. 2010. Revelle revisited: buffer factors that quantify the response of ocean chemistry to changes in DIC and alkalinity. *Glob. Biogeochem. Cycles* 24:GB1002

Ekstrom JA, Suatoni L, Cooley SR, Pendleton LH, Waldbusser GG, et al. 2015. Vulnerability and adaptation of US shellfisheries to ocean acidification. *Nat. Clim. Change* 5:207–14

Evans W, Mathis JT, Cross JN. 2014. Calcium carbonate corrosivity in an Alaskan Inland Sea. *Biogeosciences* 11:365–79

Evans W, Pocock K, Hare A, Weekes C, Hales B, et al. 2019. Marine CO_2 patterns in the northern Salish Sea. *Front. Mar. Sci.* 5:536

Fassbender AJ, Rodgers KB, Palevsky HI, Sabine CL. 2018. Seasonal asymmetry in the evolution of surface ocean pCO_2 and pH thermodynamic drivers and the influence on sea-air CO_2 flux. *Glob. Biogeochem. Cycles* 32:1476–97

Feely RA, Alin SR, Carter B, Bednaršek N, Hales B, et al. 2016. Chemical and biological impacts of ocean acidification along the west coast of North America. *Estuar. Coast. Shelf Sci.* 183:260–70

Feely RA, Alin SR, Newton JA, Sabine CL, Warner M, et al. 2010. The combined effects of ocean acidification, mixing, and respiration on pH and carbonate saturation in an urbanized estuary. *Estuar. Coast. Shelf Sci.* 88:442–49

Feely RA, Doney SC, Cooley SR. 2009. Ocean acidification: present conditions and future changes in a high-CO_2 world. *Oceanography* 22(4):36–47

Feely RA, Klinger T, Newton JA, Chadsey M, eds. 2012a. *Scientific summary of ocean acidification in Washington State marine waters*. Rep., Off. Ocean. Atmos. Res., Natl. Ocean. Atmos. Adm., Silver Spring, MD

Feely RA, Okazaki RR, Cai W-J, Bednaršek N, Alin SR, et al. 2018. The combined effects of acidification and hypoxia on pH and aragonite saturation in the coastal waters of the California current ecosystem and the northern Gulf of Mexico. *Cont. Shelf Res.* 152:50–60

Feely RA, Sabine CL, Byrne RH, Millero FJ, Dickson AG, et al. 2012b. Decadal changes in the aragonite and calcite saturation state of the Pacific Ocean. *Glob. Biogeochem. Cycles* 26:GB3001

Feely RA, Sabine CL, Hernandez-Ayon JM, Ianson D, Hales B. 2008. Evidence for upwelling of corrosive "acidified" water onto the continental shelf. *Science* 320:1490–92

Feely RA, Sabine CL, Lee K, Berelson W, Kleypas J, et al. 2004. Impact of anthropogenic CO_2 on the $CaCO_3$ system in the oceans. *Science* 305:362–66

Fennel K, Testa JM. 2019. Biogeochemical controls on coastal hypoxia. *Annu. Rev. Mar. Sci.* 11:105–30
Frankignoulle M. 1994. A complete set of buffer factors for acid-base CO_2 system in seawater. *J. Mar. Syst.* 5:111–18
Friedlingstein P, Jones MW, O'Sullivan M, Andrew RM, Hauck J, et al. 2019. Global Carbon Budget 2019. *Earth Syst. Sci. Data*. 11:1783–838
Friedman JR, Shadwick EH, Friedrichs MAM, Najjar RG, De Meo OA, et al. 2020. Seasonal variability of the CO_2 system in a large coastal plain estuary. *J. Geophys. Res. Oceans* 125:e2019JC015609
Geyer WR, MacCready P. 2014. The estuarine circulation. *Annu. Rev. Fluid Mech.* 46:175–97
Glandon HL, Miller TJ. 2017. No effect of high pCO_2 on juvenile blue crab, *Callinectes sapidus*, growth and consumption despite positive responses to concurrent warming. *ICES J. Mar. Sci.* 74:1201–9
Goodrich DM, Boicourt WC, Hamilton P, Pritchard DW. 1987. Wind-induced destratification in Chesapeake Bay. *J. Phys. Oceanogr.* 17:2232–40
Green MA, Waldbusser GG, Reilly SL, Emerson K, O'Donnell S. 2009. Death by dissolution: sediment saturation state as a mortality factor for juvenile bivalves. *Limnol. Oceanogr.* 54:1037–47
Hagens M, Slomp CP, Meysman FJR, Seitaj D, Harlay J, et al. 2015. Biogeochemical processes and buffering capacity concurrently affect acidification in a seasonally hypoxic coastal marine basin. *Biogeosciences* 12:1561–83
Hales B, Suhrbier A, Waldbusser GG, Feely RA, Newton JA. 2016. The carbonate chemistry of the "fattening line," Willapa Bay, 2011–2014. *Estuaries Coasts* 40:173–86
Halverson MJ, Bélanger C, Gay SM. 2013. Seasonal transport variations in the straits connecting Prince William Sound to the Gulf of Alaska. *Cont. Shelf Res.* 63:S63–78
Herrmann M, Najjar RG, Da F, Friedman J, Friedrichs MAM, Goldberger S. et al. 2020. Challenges in quantifying air–water carbon dioxide flux using estuarine water quality data: case study for Chesapeake Bay. *J. Geophys. Res. Oceans* 125:e2019JC015610
Hettinger A, Sanford E, Hill T, Russell A, Sato K, et al. 2012. Persistent carry-over effects of planktonic exposure to ocean acidification in the Olympia oyster. *Ecology* 93:2758–68
Hofmann AF, Middelburg JJ, Soetaert K, Meysman FJR. 2009. pH modelling in aquatic systems with time-variable acid-base dissociation constants applied to the turbid, tidal Scheldt estuary. *Biogeosciences* 6:1539–61
Hofmann AF, Soetaert K, Middelburg J, Meysman FR. 2010. AquaEnv: an aquatic acid-base modelling environment in R. *Aquat. Geochem.* 16:507–46
Hu X, Cai W-J. 2013. Estuarine acidification and minimum buffer zone—a conceptual study. *Geophys. Res. Lett.* 40:5176–81
Huang W-J, Cai W-J, Wang Y, Lohrenz SE, Murrell MC. 2015. The carbon dioxide system on the Mississippi River-dominated continental shelf in the northern Gulf of Mexico: 1. Distribution and air-sea CO_2 flux. *J. Geophys. Res. Oceans* 120:1429–45
Huang W-J, Cai W-J, Xie X, Li M. 2019. Wind-driven lateral variations of partial pressure of carbon dioxide in a large estuary. *J. Mar. Syst.* 195:67–73
Hunt CW, Salisbury JE, Vandemark D. 2011. Contribution of non-carbonate anions to total alkalinity and overestimation of pCO_2 in New England and New Brunswick rivers. *Biogeosciences* 8:3069–76
Ianson D, Allen SE, Moore-Maley BL, Johannessen SC, Macdonald RW. 2016. Vulnerability of a semienclosed estuarine sea to ocean acidification in contrast with hypoxia. *Geophys. Res. Lett.* 43:5793–801
Jansson A, Lischka S, Boxhammer T, Schulz KG, Norkko J. 2016. Survival and settling of larval *Macoma balthica* in a large-scale mesocosm experiment at different fCO_2 levels. *Biogeosciences* 12:20411–35
Jensen HS, Nielsen OI, Koch MS, de Vicentea I. 2009. Phosphorus release with carbonate dissolution coupled to sulfide oxidation in Florida Bay seagrass sediments. *Limnol. Oceanogr.* 54:1753–64
Jiang L-Q, Carter BR, Feely RA, Lauvset SK, Olsen A. 2019. Surface ocean pH and buffer capacity: past, present and future. *Sci. Rep.* 9:18624
Jiang L-Q, Feely RA, Carter BR, Greeley DJ, Gledhill DK, Arzayus KM. 2015. Climatological distribution of aragonite saturation state in the global oceans. *Glob. Biogeochem. Cycles* 29:1656–73
Jiang Z-P, Cai W-J, Chen B, Wang K, Han C, et al. 2019. Physical and biogeochemical controls on pH dynamics in the northern Gulf of Mexico during summer hypoxia. *J. Geophys. Res. Oceans* 124:5979–98

Joesoef A, Huang W-J, Gao Y, Cai W-J. 2015. Air-water fluxes and sources of carbon dioxide in the Delaware Estuary: spatial and seasonal variability. *Biogeosciences* 12:6086–101

Joesoef A, Kirchman DL, Sommerfield CK, Cai W-J. 2017. Seasonal variability of the inorganic carbon system in a large coastal plain estuary. *Biogeosciences* 14:4949–63

Kato S, Schroeter SC. 1985. Biology of the red sea urchin, *Strongylocentrotus franciscanus*, and its fishery in California. *Mar. Fish. Rev.* 47:1–20

Khangaonkar T, Sackmann B, Long W, Mohamedali T, Roberts M. 2012. Simulation of annual biogeochemical cycles of nutrient balance, phytoplankton bloom(s), and DO in Puget Sound using an unstructured grid model. *Ocean Dyn.* 62:1353–79

Kim T, Khangaonkar T. 2012. An offline unstructured biogeochemical model (UBM) for complex estuarine and coastal environments. *Environ. Model. Softw.* 31:47–63

Kwiatkowski L, Orr JC. 2018. Diverging seasonal extremes for ocean acidification during the twenty-first century. *Nat. Clim. Change* 8:141–45

Landschützer P, Gruber N, Bakker DCE, Stemmler I, Six KD. 2018. Strengthening seasonal marine CO_2 variations due to increasing atmospheric CO_2. *Nat. Clim. Change* 8:146–50

Lee DY, Owens MS, Doherty M, Eggleston EM, Hewson I, et al. 2015. The effects of oxygen transition on community respiration and potential chemoautotrophic production in a seasonally stratified anoxic estuary. *Estuaries Coasts* 38:104–17

Lewis E, Wallace D. 1998. *Program developed for CO_2 system calculations*. Rep. ORNL/CDIAC-105, Carbon Dioxide Inf. Anal. Cent., Oak Ridge Natl. Lab., Oak Ridge, TN

Li M, Zhong L, Boicourt WC. 2005. Simulations of Chesapeake Bay estuary: sensitivity to turbulence mixing parameterizations and comparison with observations. *J. Geophys. Res. Oceans* 110:C12004

Loesch H. 1960. Sporadic mass shoreward migrations of demersal fish and crustaceans in Mobile Bay, Alabama. *Ecology* 41:292–98

Long WC, Swiney KM, Foy RJ. 2013a. Effects of ocean acidification on the embryos and larvae of red king crab, *Paralithodes camtschaticus*. *Mar. Pollut. Bull.* 69:38–47

Long WC, Swiney KM, Harris C, Page HN, Foy RJ. 2013b. Effects of ocean acidification on juvenile red king crab (*Paralithodes camtschaticus*) and Tanner crab (*Chionoecetes bairdi*) growth, condition, calcification, and survival. *PLOS ONE* 8:e60959

Masson D. 2006. Seasonal water mass analysis for the Straits of Juan de Fuca and Georgia. *Atmos. Ocean* 44:1–15

Mathis JT, Cooley SR, Lucey N, Colt S, Ekstrom J, et al. 2015. Ocean acidification risk assessment for Alaska's fishery sector. *Prog. Oceanogr.* 136:71–91

McNeil BI, Sasse TP. 2016. Future ocean hypercapnia driven by anthropogenic amplification of the natural CO_2 cycle. *Nature* 529:383–86

Mearns LO, Sain S, Leung LR, Bukovsky MS, McGinnis S, et al. 2013. Climate change projections of the North American Regional Climate Change Assessment Program (NARCCAP). *Clim. Change* 120:965–75

Middelburg JJ, Soetaert K, Hagens M. 2020. Ocean alkalinity, buffering and biogeochemical processes. *Rev. Geophys.* 58:e2019RG000681

Miller AW, Reynolds AC, Sobrino C, Riedel GF. 2009. Shellfish face uncertain future in high CO_2 world: influence of acidification on oyster larvae calcification and growth in estuaries. *PLOS ONE* 4:e5661

Miller J, Maher M, Bohaboy E, Friedman C, McElhany P. 2016. Exposure to low pH reduces survival and delays development in early life stages of Dungeness crab (*Cancer magister*). *Mar. Biol.* 163:118

Millero FJ. 1991. The oxidation of H_2S in the Chesapeake Bay. *Estuar. Coast. Shelf Sci.* 33:521–27

Moore SK, Mantua NJ, Newton JA, Kawase M, Warner MJ, Kellogg JP. 2008. A descriptive analysis of temporal and spatial patterns of variability in Puget Sound oceanographic properties. *Estuar. Coast. Shelf Sci.* 80:545–54

Moore-Maley BL, Allen SE, Ianson D. 2016. Locally driven interannual variability of near-surface pH and Ω_A in the Strait of Georgia. *J. Geophys. Res. Oceans* 121:1600–25

Mucci A. 1983. The solubility of calcite and aragonite in seawater at various salinity, temperatures, and one atmosphere total pressure. *Am. J. Sci.* 283:789–99

Müller JD, Rehder G. 2018. Metrology of pH measurements in brackish waters—part 2: experimental characterization of purified meta-Cresol Purple for spectrophotometric pH_T measurements. *Front. Mar. Sci.* 5:177

Musgrave DL, Halverson MJ, Pegau WS. 2013. Seasonal surface circulation, temperature, and salinity in Prince William Sound, Alaska. *Cont. Shelf Res.* 53:20–29

Najjar RG, Herrmann M, Cintrón Del Valle SM, Friedman JR, Friedrichs MAM, et al. 2020. Alkalinity in tidal tributaries of the Chesapeake Bay. *J. Geophys. Res. Oceans* 125:e2019JC015597

Natl. Geophys. Data Cent. 2009. *Prince William Sound, Alaska 8/3 Arc-second MHHW Coastal Digital Elevation Model*. Data Set, Natl. Geophys. Data Cent., Natl. Ocean. Atmos. Adm., Silver Spring, MD

Neal EG, Hood E, Smikrud K. 2010. Contribution of glacier runoff to freshwater discharge into the Gulf of Alaska. *Geophys. Res. Lett.* 37:L06404

Ni W, Li M, Ross AC, Najjar RG. 2019. Large projected decline in dissolved oxygen in a eutrophic estuary due to climate change. *J. Geophys. Res. Oceans* 124:8271–89

Orr JC, Fabry VJ, Aumont O, Bopp L, Doney SC, et al. 2005. Anthropogenic ocean acidification over the twenty-first century and its impact on calcifying organisms. *Nature* 437:681–86

Pacella SR, Brown CA, Waldbusser GG, Labiosa RG, Hales B. 2018. Seagrass habitat metabolism increases short-term extremes and long-term offset of CO_2 under future ocean acidification. *PNAS* 115:3870–75

Pawlowicz R, Riche O, Halverson M. 2007. The circulation and residence time of the Strait of Georgia using a simple mixing-box approach. *Atmos. Ocean* 45:173–93

Pelletier G, Roberts M, Keyzers M, Alin SR. 2018. Seasonal variation in aragonite saturation in surface waters of Puget Sound – a pilot study. *Elem. Sci. Anthr.* 6:5

Perez FF, Fontela M, García-Ibáñez MI, Mercier H, Velo A, et al. 2018. Meridional overturning circulation conveys fast acidification to the deep Atlantic Ocean. *Nature* 554:515–18

Pierrot D, Lewis E, Wallace D. 2006. *MS Excel program developed for CO_2 system calculations*. Rep., ORNL/CDIAC-105a, Carbon Dioxide Inf. Anal. Cent., Oak Ridge Natl. Lab., Oak Ridge, TN

Reuter KE, Lotterhos KE, Crim RN, Thompson CA, Harley CD. 2011. Elevated pCO_2 increases sperm limitation and risk of polyspermy in the red sea urchin *Strongylocentrotus franciscanus*. *Glob. Change Biol.* 17:163–71

Riahi K, Rao S, Krey V, Cho C, Chirkov V, et al. 2011. RCP 8.5—a scenario of comparatively high greenhouse gas emissions. *Clim. Change* 109:33–57

Riebesell U, Gattuso J-P. 2014. Lessons learned from ocean acidification research. *Nat. Clim. Change* 5:12–14

Ries JB, Cohen AL, McCorkle DC. 2009. Marine calcifiers exhibit mixed responses to CO_2-induced ocean acidification. *Geology* 37:1131–34

Roden EE, Tuttle JH. 1992. Sulfide release from estuarine sediments underlying anoxic bottom water. *Limnol. Oceanogr.* 37:725–38

Saba GK, Goldsmith KA, Cooley SR, Grosse D, Meseck SL, et al. 2019. Recommended priorities for research on ecological impacts of ocean and coastal acidification in the U.S. Mid-Atlantic. *Estuar. Coast. Shelf Sci.* 225:106188

Sabine CL, Feely RA, Key RM, Bullister JL, Millero FJ, et al. 2002. Distribution of anthropogenic CO_2 in the Pacific Ocean. *Glob. Biogeochem. Cycles* 16:30-1–17

Salisbury J, Green M, Hunt C, Campbell J. 2008. Coastal acidification by rivers: a threat to shellfish? *Eos Trans. AGU* 89:513

Sanford L, Sellner K, Breitburg D. 1990. Covariability of dissolved oxygen with physical processes in the summertime Chesapeake Bay. *J. Mar. Res.* 48:567–90

Scully ME. 2010. Wind modulation of dissolved oxygen in Chesapeake Bay. *Estuaries Coasts* 33:1164–75

Scully ME, Friedrichs C, Brubaker J. 2005. Control of estuarine stratification and mixing by wind-induced straining of the estuarine density field. *Estuaries* 28:321–26

Sharp JH. 2010. Estuarine oxygen dynamics: What can we learn about hypoxia from long-time records in the Delaware Estuary? *Limnol. Oceanogr.* 55:535–548

Sharp JH, Yoshiyama K, Parker A, Schwartz M, Curless S, et al. 2009. A biogeochemical view of estuarine eutrophication: seasonal and spatial trends and correlations in the Delaware estuary. *Estuaries Coasts* 32:1023–43

Shen C, Testa JM, Li M, Cai W-J. 2020. Understanding anthropogenic impacts on pH and aragonite saturation state in Chesapeake Bay: insights from a 30-year model study. *J. Geophys. Res. Biogeosci.* 125:e2019JG005620

Shen C, Testa JM, Li M, Cai W-J, Waldbusser GG, et al. 2019a. Controls on carbonate system dynamics in a coastal plain estuary: a modeling study. *J. Geophys. Res. Biogeosci.* 124:61–78

Shen C, Testa JM, Ni W, Cai W-J, Li M, Kemp WM. 2019b. Ecosystem metabolism and carbon balance in Chesapeake Bay: a 30-year analysis using a coupled hydrodynamic-biogeochemical model. *J. Geophys. Res. Oceans* 124:6141–53

Sommerfield C, Wong K-C. 2011. Mechanisms of sediment flux and turbidity maintenance in the Delaware Estuary. *J. Geophys. Res. Oceans* 116:C01005

Song S, Wang ZA, Gonneea ME, Kroeger KD, Chu SN, et al. 2020. An important biogeochemical link between organic and inorganic carbon cycling: effects of organic alkalinity on carbonate chemistry in coastal waters influenced by intertidal salt marshes. *Geochim. Cosmochim. Acta* 275:123–39

Stabeno PJ, Bond NA, Hermann AJ, Kachel NB, Mordy CW, Overland JE. 2004. Meteorology and oceanography of the Northern Gulf of Alaska. *Cont. Shelf Res.* 24:859–97

St-Laurent P, Friedrichs MAM, Najjar RG, Shadwick EH, Tian H, et al. 2020. Relative impacts of global changes and regional watershed changes on the inorganic carbon balance of the Chesapeake Bay. *Biogeosciences* 17:3779–96

Su J, Cai W-J, Brodeur J, Chen B, Hussain N, et al. 2020a. Chesapeake Bay acidification buffered by spatially-decoupled carbonate mineral cycling. *Nat. Geosci.* 13:441–47

Su J, Cai W-J, Brodeur J, Hussain N, Chen B, et al. 2020b. Source partitioning of oxygen-consuming organic matter in the hypoxic zone of the Chesapeake Bay. *Limnol. Oceanogr.* 65:1801–17

Sunda WG, Cai W-J. 2012. Eutrophication induced CO_2-acidification of subsurface coastal waters: interactive effects of temperature, salinity, and atmospheric P_{CO_2}. *Environ. Sci. Technol.* 46:10651–59

Sutherland D, MacCready P, Banas N, Smedstad L. 2011. A model study of the Salish Sea estuarine circulation. *J. Phys. Oceanogr.* 41:1125–43

Takahashi T, Olafsson J, Goddard JG, Chipman DW, Sutherland SC. 1993. Seasonal variation of CO_2 and nutrients in the high-latitude surface oceans: a comparative study. *Glob. Biogeochem. Cycles* 7:843–78

Takahashi T, Sutherland SC, Chipman DW, Goddard JG, Ho C, et al. 2014. Climatological distributions of pH, pCO_2, total CO_2, alkalinity, and $CaCO_3$ saturation in the global surface ocean, and temporal changes at selected locations. *Mar. Chem.* 164:95–125

Takeshita Y, Frieder CA, Martz TR, Ballard JR, Feely RA, et al. 2015. Including high-frequency variability in coastal ocean acidification projections. *Biogeosciences* 12:5853–70

Talmage SC, Gobler CJ. 2009. The effects of elevated carbon dioxide concentrations on the metamorphosis, size, and survival of larval hard clams (*Mercenaria mercenaria*), bay scallops (*Argopecten irradians*), and eastern oysters (*Crassostrea virginica*). *Limnol. Oceanogr.* 54:2072–80

Testa JM, Murphy RR, Brady DC, Kemp WM. 2018. Nutrient- and climate-induced shifts in the phenology of linked biogeochemical cycles in a temperate estuary. *Front. Mar. Sci.* 5:114

Thrush S, Townsend M, Hewitt J, Davies K, Lohrer A, et al. 2014. The many uses and values of estuarine ecosystems. In *Ecosystem Services in New Zealand: Conditions and Trends*, ed. JR Dymond, pp. 226–37. Lincoln, N.Z.: Manaaki Whenua

Tomanek L, Zuzow MJ, Ivanina AV, Beniash E, Sokolova IM. 2011. Proteomic response to elevated P_{CO_2} level in eastern oysters, *Crassostrea virginica*: evidence for oxidative stress. *J. Exp. Biol.* 214:1836–44

Van Dam BR, Wang H. 2019. Decadal-scale acidification trends in adjacent North Carolina estuaries: competing role of anthropogenic CO_2 and riverine alkalinity loads. *Front. Mar. Sci.* 6:136

Völker C, Wallace DWR, Wolf-Gladrow DA. 2002. On the role of heat fluxes in the uptake of anthropogenic carbon in the North Atlantic. *Glob. Biogeochem. Cycles* 16:85–89

Waldbusser GG, Hales B, Langdon CJ, Haley BA, Schrader P, et al. 2015a. Ocean acidification has multiple modes of action on bivalve larvae. *PLOS ONE* 10:e0128376

Waldbusser GG, Hales B, Langdon CJ, Haley BA, Schrader P, et al. 2015b. Saturation-state sensitivity of marine bivalve larvae to ocean acidification. *Nat. Clim. Change* 5:273–80

Waldbusser GG, Salisbury JE. 2014. Ocean acidification in the coastal zone from an organism's perspective: multiple system parameters, frequency domains, and habitats. *Annu. Rev. Mar. Sci.* 6:221–47

Waldbusser GG, Voigt E, Bergschneider H, Green M, Newell RE. 2011. Biocalcification in the Eastern Oyster (*Crassostrea virginica*) in relation to long-term trends in Chesapeake Bay pH. *Estuaries Coasts* 34:221–31

Wallace RB, Baumann H, Grear JS, Aller RC, Gobler CJ. 2014. Coastal ocean acidification: the other eutrophication problem. *Estuar. Coast. Shelf Sci.* 148:1–13

Wang Y, Van Cappellen P. 1996. A multicomponent reaction transport model of early diagenesis: application to redox cycling in coastal marine sediments. *Geochim. Cosmochim. Acta* 60:2993–3014

Weingartner TJ, Danielson SL, Royer TC. 2005. Freshwater variability and predictability in the Alaska Coastal Current. *Deep-Sea Res. II* 52:169–91

Xie X, Li M. 2018. Effects of wind straining on estuarine stratification: a combined observational and modeling study. *J. Geophys. Res. Oceans* 123:2363–80

Xie X, Li M, Boicourt WC. 2017. Baroclinic effects on wind-driven lateral circulation in Chesapeake Bay. *J. Phys. Oceanogr.* 47:433–45

Xu Y, Pierrot D, Cai W-J. 2017. Ocean carbonate system computation for anoxic waters using an updated CO2SYS program. *Mar. Chem.* 195:90–93

Xue Z, He R, Fennel K, Cai W-J, Lohrenz S, et al. 2016. Modeling pCO_2 variability in the Gulf of Mexico. *Biogeosciences* 13:4359–77

Yao W, Millero FJ. 1995. The chemistry of the anoxic waters in the Framvaren Fjord, Norway. *Aquat. Geochem.* 1:53–88

Zopfi J, Ferdelman TG, Jørgensen BB, Teske A, Thamdrup B. 2001. Influence of water column dynamics on sulfide oxidation and other major biogeochemical processes in the chemocline of Mariager Fjord (Denmark). *Mar. Chem.* 74:29–51